CALIBRATION

of the

ELECTRON-PROTON SPECTROMETER

LEC Document Number EPS-956

Prepared by

Lockheed Electronics Company, Inc.
Houston Aerospace Systems Division
Houston, Texas

Under Contract NAS 9-11373

For

National Aeronautics and Space Administration
Manned Spacecraft Center
Houston, Texas

[1972]

CALIBRATION

of the

ELECTRON-PROTON SPECTROMETER

LEC Document Number EPS-956

Prepared by

Lockheed Electronics Company, Inc.
Houston Aerospace Systems Division
Houston, Texas

Under Contract NAS 9-11373

For

National Aeronautics and Space Administration
Manned Spacecraft Center
Houston, Texas

CALIBRATION

of the

ELECTRON-PROTON SPECTROMETER

Prepared by: B. L. Cash
B. L. Cash
Staff Engineer

Approved by: B. E. Curtsinger
B. E. Curtsinger
Engineering Supervisor

Approved by: B C Hall
B. C. Hall
Program Manager

Lockheed Electronics Company, Inc.
Houston Aerospace Systems Division
Houston, Texas

Preface

This report was prepared under NASA Contract NAS 9-11373 for the Electron-Proton Spectrometer (EPS) for Skylab.

Reported herein are the results of a calibration program to determine a suitable analytic method to determine the proton response functions, and to determine experimentally both the proton and electron response functions.

TABLE OF CONTENTS

1.0 INTRODUCTION

The principal function of the sensor used in the Electron-Proton Spectrometer (EPS) is to provide a signal which can be used to determine the energy and indicate the type of an incident particle. Two techniques are employed to resolve the particle intensity in different energy regions. The first employs a moderator surrounding each detector to provide a nominal lower limit to the energy of a particle which can be detected. The second technique utilizes a pulse height discriminator to identify those particles entering a detector whose energy is (1) sufficiently high that it exceeds the discriminator level if the particle is stopped in the detector, or (2) sufficiently low that the ionization rate causes the discrimination level to be exceeded for paths through the detector shorter than the particle range. For a unique pathlength through the detector, e.g. normal to any face, these criteria select an energy range for any one particle type, with the definition of the energy boundaries limited principally by straggling and scattering. The wide distribution of pathlengths through a cubical detector permits a wider energy range for which both criteria can be satisfied, since a different energy range is associated with each particular pathlength sample. As a result, the boundaries of the "nominal" energy range are not distinct, and the performance of each energy channel must be described by a probability function which describes the probability of exceeding the discriminator level versus the particle energy.

1.0 Continued

It is readily apparent that utilization of the data from the EPS sensors requires an accurate knowledge of these probability functions, or response functions. Two methods are available to determine response functions: analytic and experimental. From the standpoint of cost and accuracy, it is desirable to combine the two methods, combining the completeness of the analytic method with the accuracy of the experimental method. This combination approach required that computer techniques be developed to describe the specific problem which could then be verified by experimental measurements.

The purpose of this document is to describe the selected sensor design, the analytic method used to determine the sensor response functions, and the experimental verification of the calculational technique.

2.0 SENSOR DESIGN

The sensors for the EPS consist of five shielded solid state detectors. The detectors are made of lithium-drifted silicon, are cubical in shape, and are nominally 2.0 mm on each side. The detectors are each contained in a hemispherical shield of aluminum or brass. The basic design concept of the EPS requires that one electron level and one proton level be measured with each of four shielded detectors. The fifth shielded detector is used to determine the highest proton

2.0 Continued

level. The dual role of each of the first four sensors is achieved through the use of two discriminator levels; one is low enough, i.e. 200 keV, to count both electrons and protons, and the other is high enough, i.e. 2.0 MeV, to discriminate against electrons while still counting a large percentage of the protons and minimizing the impact of an anomalous pulse height distribution, Figure 1, which occurs for many of the detectors. The fifth sensor also has two discriminator levels, viz 2.0 MeV and 1.0 MeV, but both are used to count protons. The energy threshold of each channel is controlled through the selection of the shield thickness. The final shield thicknesses are given in Table I.

Table I Shield Thicknesses

Channel	Shield Thickness (cm) Mat'l	Nominal Threshold Proton	Electron
1	.037 Al	8.0 MeV	.54 MeV
2	.180 Al	18.5	1.48
3	.280	23.6	1.98
4	.710 Al	39.7	4.28
5	.890 Br	77.0	--

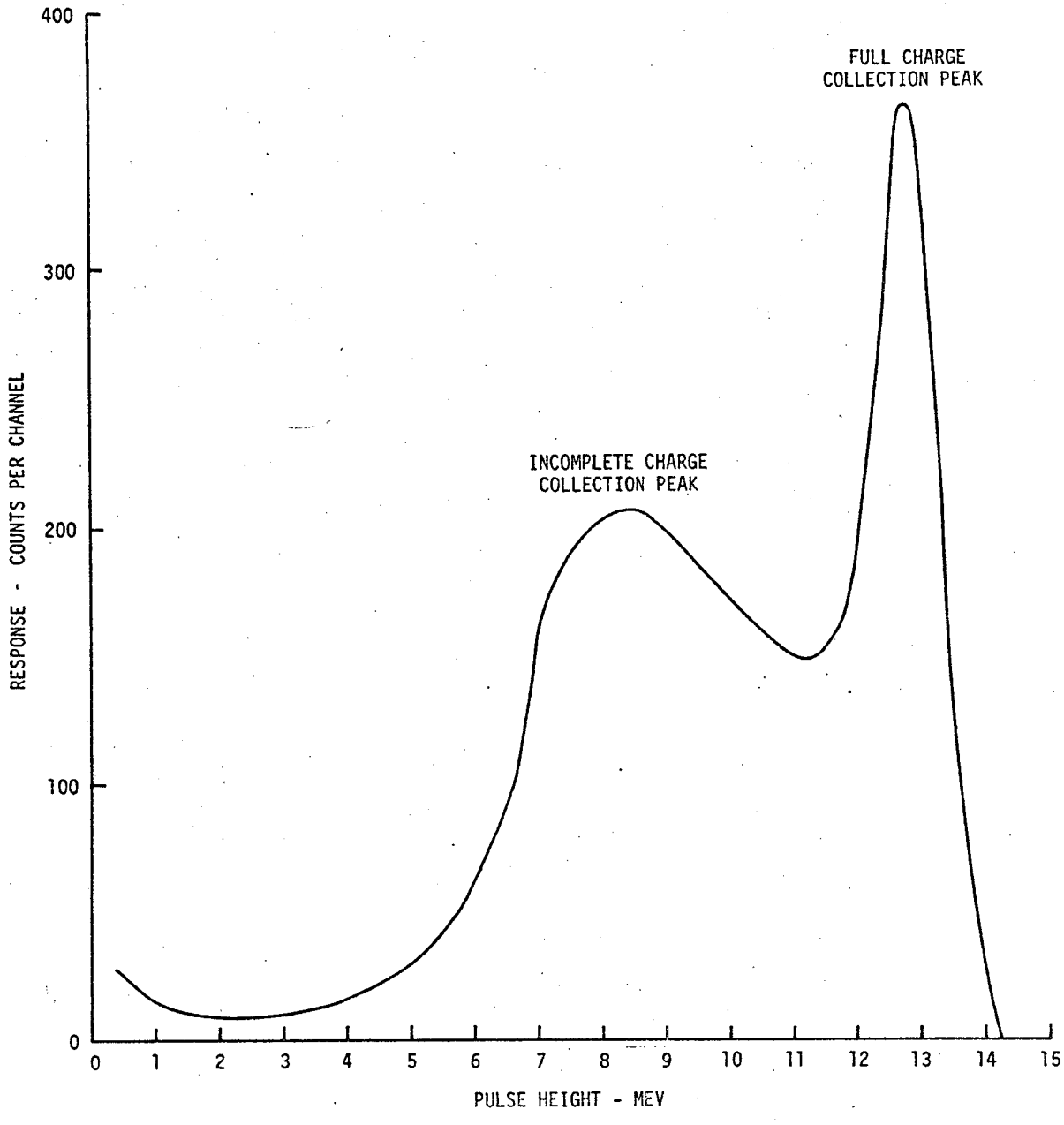

Figure 1. — Anomalous Pulse Height Distribution of a 2.0 mm Cubical Detector Exposed to 21.6 MEV Protons Normal to the Top Surface.

2.0 Continued

The proton discriminator setting of 2.0 MeV was dictated by the discovery of the anomalous pulse height distribution, Figure 1, present to various degrees for most of the cubical detectors. The effect was discovered while using penetrating protons from a cyclotron to determine the depletion depth of some of the detectors undergoing screening and testing. In the experiment, uncollimated protons of 21.6 MeV were allowed to impinge on the top surface of the detectors, normal to the detector surface. The resulting pulse height distribution should contain a single peak, the energy of which should be characteristic of the depletion depth of the detector. In many of the detectors a lower energy pulse distribution also occurred, which would indicate incomplete charge collection for many of the pulses. Typically, the peak value for the anomaly occurred at approximately 2/3 the normal peak value. The percentage of pulses under the anomaly varied from detector to detector and, unfortunately, from time to time in the same detector. The magnitude of the anomaly is worst for barely penetrating protons and decreases for increasing proton energy. In a few detectors the anomaly was hardly discernable while in others it was so large the primary peak was indiscernable to the extent that the active depth of the detector could not be determined from energy deposition of penetrating protons. The curve in Figure 1 is typical of the better quality anomalous detectors, i.e. those few with an even better response showed no anomaly at all. Relative to a detector with no anomaly, the better quality anomalous detectors had 30 - 40% of their pulses under the anomaly peak, where the anomaly peak is the remainder after a normalized good response is subtracted. Detectors were observed to change from 0% anomaly to about 40% and from 30% to about 60%.

2.0 Continued

A detector testing program had been undertaken in order to screen the detectors and to develop a means to estimate their reliability. The testing program extended over several months and involved approximately 100 detectors, with various degrees of involvement. It was determined, among other things, that the quality of the surviving detectors improved or deteriorated in an apparently unpredictable fashion.

In view of the inability to predict the quality of the detectors, it was necessary to devise a method of operation that would circumvent the problem. It was determined that using detectors of this type in a differential spectrometer mode, as several experimenters have, and hence with high discriminator levels, would result in unacceptably high errors in the resulting count rate. Use of a high discriminator level, e.g. 4 - 8 MeV, results in a substantial loss of counts under the anomaly peak at higher proton energies. For example, with a discriminator setting of 6.0 MeV and a primary peak energy of 9 MeV, all of the anomaly counts would be lost, giving rise to a substantial error in total counts. As a result of such losses, errors of 30 - 50% can be incurred in channel count rates calculated for a typical proton spectrum such as expected to be encountered by Skylab. The manufacturer and other experimenters using this type of detector were contacted to see how they had circumvented the problem. No one could be located who had tested their detectors so as to determine the existence of the anomaly. Subsequent testing on the part of some showed that they, too, had the problem. Additional experimental work and subsequent analysis showed that the problem could be virtually eliminated by operating the spectrometer in a pseudo integral mode utilizing discriminator levels of 2.0 MeV. This level was chosen as a compromise between electron contamination and proton response. The impact of the residual detector variances on system error is discussed in section 4.2.

3.0 ANALYTIC DETERMINATION OF RESPONSE FUNCTIONS

The count rate, r, of a detector can be related to the incident flux, Φ, by the expression

$$r/\Phi = \varepsilon\, G$$

Where ε is the counting efficiency of the detector and is defined as the fraction of particles with energy E striking the detector that are recorded, and G is the geometric or area factor.

The geometric factor for a near cubical detector with dimensions L_X, L_Y, and L_Z, with a 2π steradian acceptance angle can be calculated by looking at each face separately. The geometric factor of the top face area is given by

$$g_t = \frac{1}{4\pi} \int_0^{\pi/2} \int_0^{2\pi} L_X\, L_Y \sin\alpha \cos\alpha \, d\alpha \, d\phi$$

$$= L_X\, L_Y/4$$

where α and ϕ are the angles of incidence in spherical coordinates. Similarly a typical side has the factor

$$g_{s_1} = \frac{1}{4\pi} \int_0^{\pi/2} \int_0^{\pi} L_X\, L_Y \cos\alpha \sin\alpha \, d\alpha \, d\phi$$

$$= L_X\, L_Z/8,$$

or, for the four sides

$$g_s = \frac{1}{4} \; (L_X\, L_Z + L_Y\, L_Z).$$

3.0 Continued

The total geometric factor, G, is simply the sum of the factors for the five exposed faces

$$G = g_t + g_s$$

$$= \frac{1}{4} (L_X L_Y + L_X L_Z + L_Y L_Z)$$

Assuming straight line penetration of the particle through the detecfor, as is approximately the case for protons, and letting m(E) be the pathlength necessary to deposit an amount of energy equal to the discriminator threshold, a portion of the detector will be ineffective for producing counts because of corner cutting and penetration of the detector by m(E). Now considering those losses where the track starts at the top and ends in a side. The area involved is given by

$$a = (L - m \cos \alpha \sin \phi) \ (m \cos \alpha \cos \phi)$$

and the geometric factor lost

$$g_l = \frac{1}{4\pi} \int_0^{\pi/2} \int_0^{\pi/2} 2(L - m \cos \alpha \sin \phi) \ (m \cos \alpha \cos \phi) \ (\sin \alpha \cos \alpha) \ d\alpha \ d\phi$$

where the integration over ϕ is taken only through one quadrant and then doubled.

3.0 Continued

$$g_1 = \frac{1}{4\pi} \int_0^{\pi/2} \int_0^{\pi/2} 2\left[Lm \cos^2 \alpha \sin \alpha \cos \phi - m^2 \cos^3 \alpha \sin \alpha \sin \phi \cos \phi\right] \, d\alpha \, d\phi$$

Integrating and reducing gives

$$g_1 = \frac{1}{4\pi} \left[\frac{2}{3} Lm - \frac{m^2}{4}\right] .$$

This factor applies for each of the four top edges, each of the four bottom edges, and each of the four side edges giving consideration to the symmetry and 2π response. Thus the geometric factor lost by edge cutting is given by

$$g_1 = \frac{1}{4\pi} \left[\frac{4}{3} L_X m + \frac{4}{3} L_Y m - \frac{4m^2}{4}\right] + \frac{1}{4\pi} \left[\frac{4}{3} L_X m + \frac{4}{3} L_Y m - \frac{4m^2}{4}\right] + \frac{1}{4\pi} \left[\frac{8}{3} L_Z m - \frac{4m^2}{4}\right]$$

$$g_1 = \frac{1}{\pi} \left[\frac{2}{3} L_X m + \frac{2}{3} L_Y m + \frac{2}{3} L_Z m - \frac{3}{4} m^2\right]$$

Since this factor represents lost area, it must be subtracted from the total surface factor.
Thus for $m < L$,

$$G - g_{1'} = \frac{1}{\pi} \left[\frac{\pi}{4} L_X L_Y + \frac{\pi}{4} L_X L_Z + \frac{\pi}{4} L_Y L_Z - \frac{2}{3} L_X m - \frac{2}{3} L_Y m - \frac{2}{3} L_Z m + \frac{3}{4} m^2\right] .$$

3.0 Continued

The edge losses also apply where $m \geq L$ providing the path begins and ends in adjacent faces. Determining the total loss for $m \geq L$ requires only the addition of losses through opposite faces. Consider first the case of particles passing from top to bottom. Those particles incident with $\alpha < \cos^{-1} \frac{L_Z}{m}$ will be lost, since the pathlength in the detector will be less than m. Now for one quadrant of ϕ, the lost area is given by

$$\frac{1}{4\pi} \int_0^{\lambda_m} \int_0^{\pi/2} (L_X - m \sin\alpha \cos\phi)\ (L_Y - m \sin\alpha \sin\phi)\ (\cos\alpha \sin\alpha)\ d\alpha\ d\phi$$

where $\lambda_m = \cos^{-1} \frac{L_Z}{m}$.

Symmetry will give the same for each quadrant of ϕ, hence multiplying by four gives the total geometric factor lost in the top face.

$$g_t = \frac{1}{\pi} \int_0^{\lambda_m} \int_0^{\pi/2} \Big| L_X L_Y \cos\alpha \sin\alpha - L_X m \sin^2\alpha \sin\phi - L_Y m \sin^2\alpha \cos\phi \cos\alpha + m^2 \sin^3\alpha \sin\phi \cos\phi \cos\alpha \Big|\ d\alpha\ d\phi$$

3.0 Continued

Integrating and collecting terms

$$g_t = \frac{1}{\pi}\left[\frac{\pi}{4} L_X L_Y \sin^2 \lambda_m - L_X m \frac{\sin^3 \lambda_m}{3} - L_Y m \frac{\sin^3 \lambda_m}{3} + \frac{m^2}{8} \sin^4 \lambda_m\right] .$$

Similarly the other faces give

$$g_{s_1} = \frac{1}{\pi}\left[\frac{\pi}{4} L_Y L_Z \sin^2 \theta_m - L_Y m \frac{\sin^3 \theta_m}{3} - L_Z m \frac{\sin^3 \theta_m}{3} + \frac{m^2}{8} \sin^4 \theta_m\right]$$

and

$$g_{s_2} = \frac{1}{\pi}\left[\frac{\pi}{4} L_X L_Z \sin^2 \delta_m - L_X m \frac{\sin^3 \delta_m}{3} - L_Z m \frac{\sin^3 \delta_m}{3} + \frac{m^2}{8} \sin^4 \delta_m\right]$$

where $\theta_m = \cos^{-1} \frac{L_X}{m}$

$\delta_m = \cos^{-1} \frac{L_Y}{m}$.

Summarizing, the total geometric factor is

$$\varepsilon G(E) = \frac{1}{\pi}\left[\frac{\pi}{4} L_X L_Y + \frac{\pi}{4} L_X L_Z + \frac{\pi}{4} L_Y L_Z - \frac{2}{3} L_X m - \frac{2}{3} L_Y m - \frac{2}{3} L_Z m + \frac{3}{4} m^2 - \frac{\pi}{4} L_X L_Y \sin^2 \lambda_m + L_X m \frac{\sin^3 \lambda_m}{3} + L_Y m \frac{\sin^3 \lambda_m}{3} - m^2 \frac{\sin^4 \lambda_m}{8}\right]$$

3.0 Continued

$$- \frac{\pi}{4} L_Y L_Z \sin^2 \theta_m + L_Y m \frac{\sin^3 \theta_m}{3} + L_Z m \frac{\sin^3 \theta_m}{3}$$

$$- m^2 \frac{\sin^4 \theta_m}{8} - \frac{\pi}{4} L_X L_Z \sin^2 \delta_m + L_X m \frac{\sin^3 \delta_m}{3}$$

$$+ L_Z m \frac{\sin^3 \delta_m}{3} - m^2 \frac{\sin^4 \delta_m}{8} \Bigg]$$

where $\cos \lambda_m = \frac{L_Z}{m}$; $\lambda_m = 0$ if $L_Z \geq m$

$\cos \theta_m = \frac{L_X}{m}$; $\theta_m = 0$ if $L_X \geq m$

$\cos \delta_m = \frac{L_Y}{m}$; $\delta_m = 0$ if $L_Y \geq m$.

The value of m(E) is determined from the range-energy tables for protons from the relation

$$m(E) = R(E) - R(E - E_B)$$

where R is the proton range and E_B is the energy equivalent of the discriminator bias level. The equation for $\varepsilon G(E)$ gives the geometric factor, i.e. response function, for an unshielded detector. The response function for a shielded detector can be determined through the transformation to a new energy coordinate (E') through the relation

$$R(E') = R(E) + \Delta R$$

where, again, R is the proton range and ΔR is the thickness of the detector shield.

3.0 Continued

A computer program has been developed which utilizes the above relationships to calculate the proton response functions for the various EPS channels. The results of these calculations are shown in Figures 2 - 7. The curves give the responses for two values of detector dimensions, for a nominal 2.0 mm cube and for L_Z increased to 2.2 mm.

Note that the knee in the curves, e.g. at 155 MeV in Figure 2, occurs at the energy for which m equals the dimension of the detector. Also note that the ratio of the two curves below the knee is very close to the ratio of the exposed surface areas of the two detectors.

No attempt was made to develop a similar program to calculate the response functions for the electrons because of the complexity of the electron scattering problem.

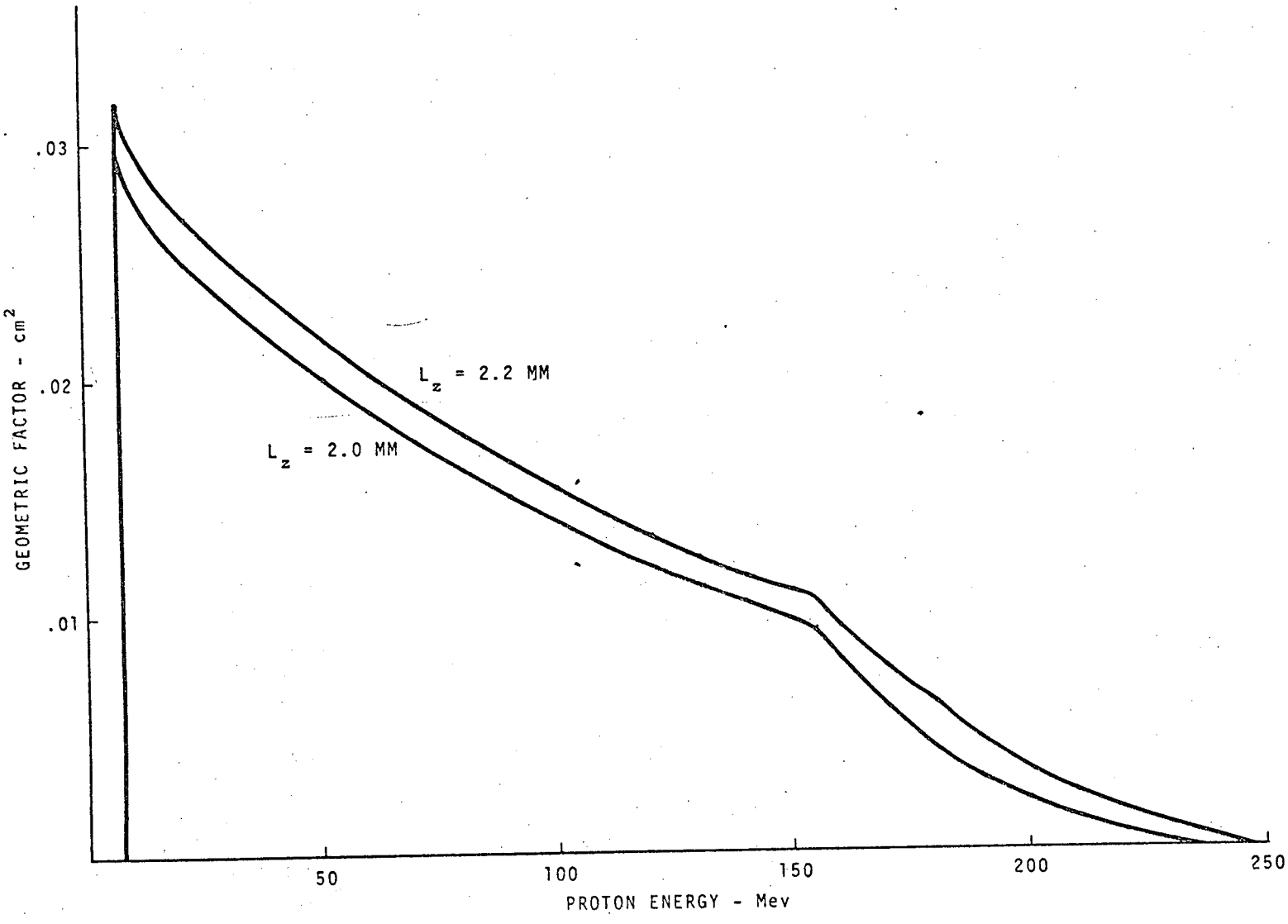

Figure 2. — Geometric Factor, Channel 1, Protons.

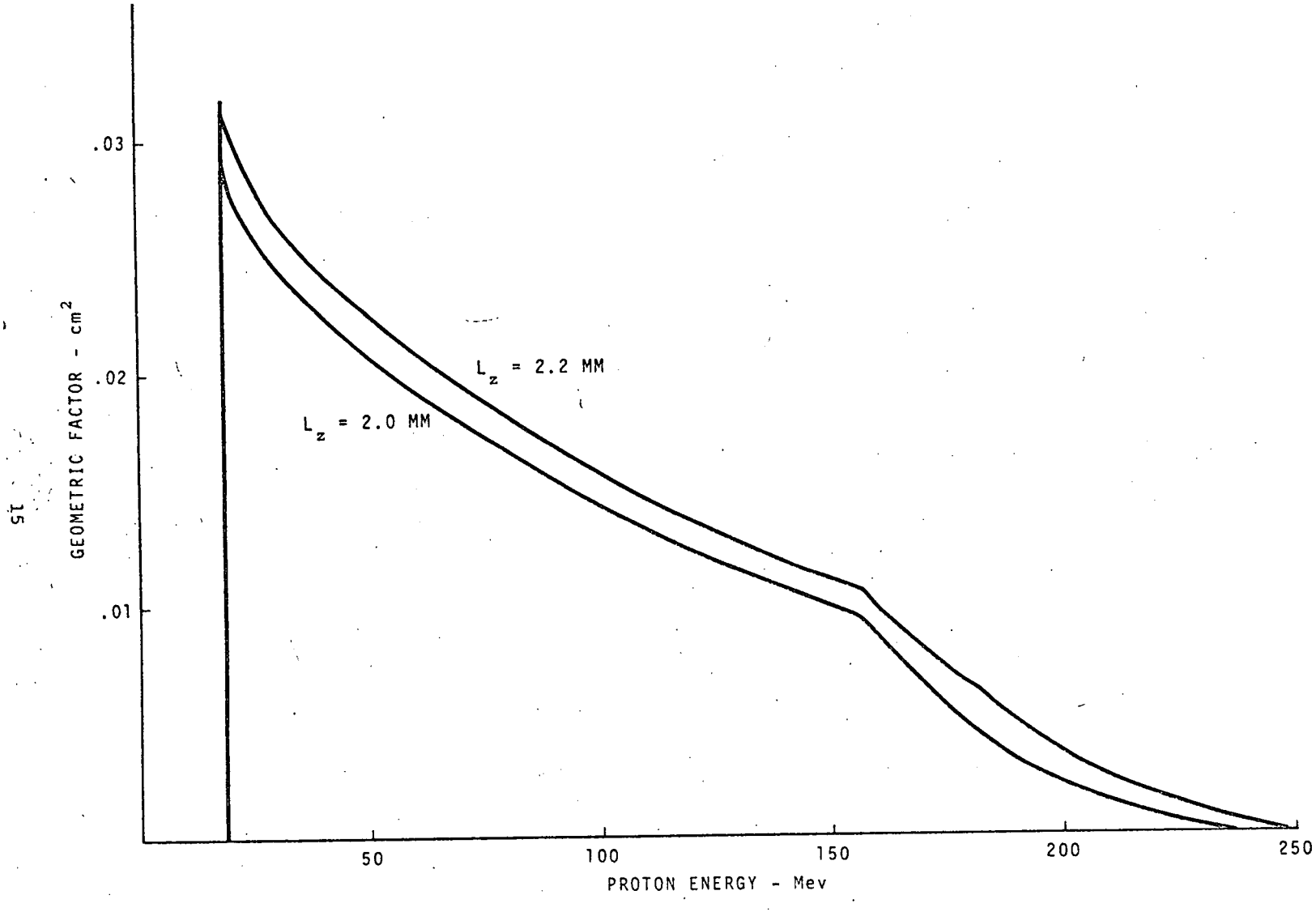

Figure 3. — Geometric Factor, Channel 2, Protons.

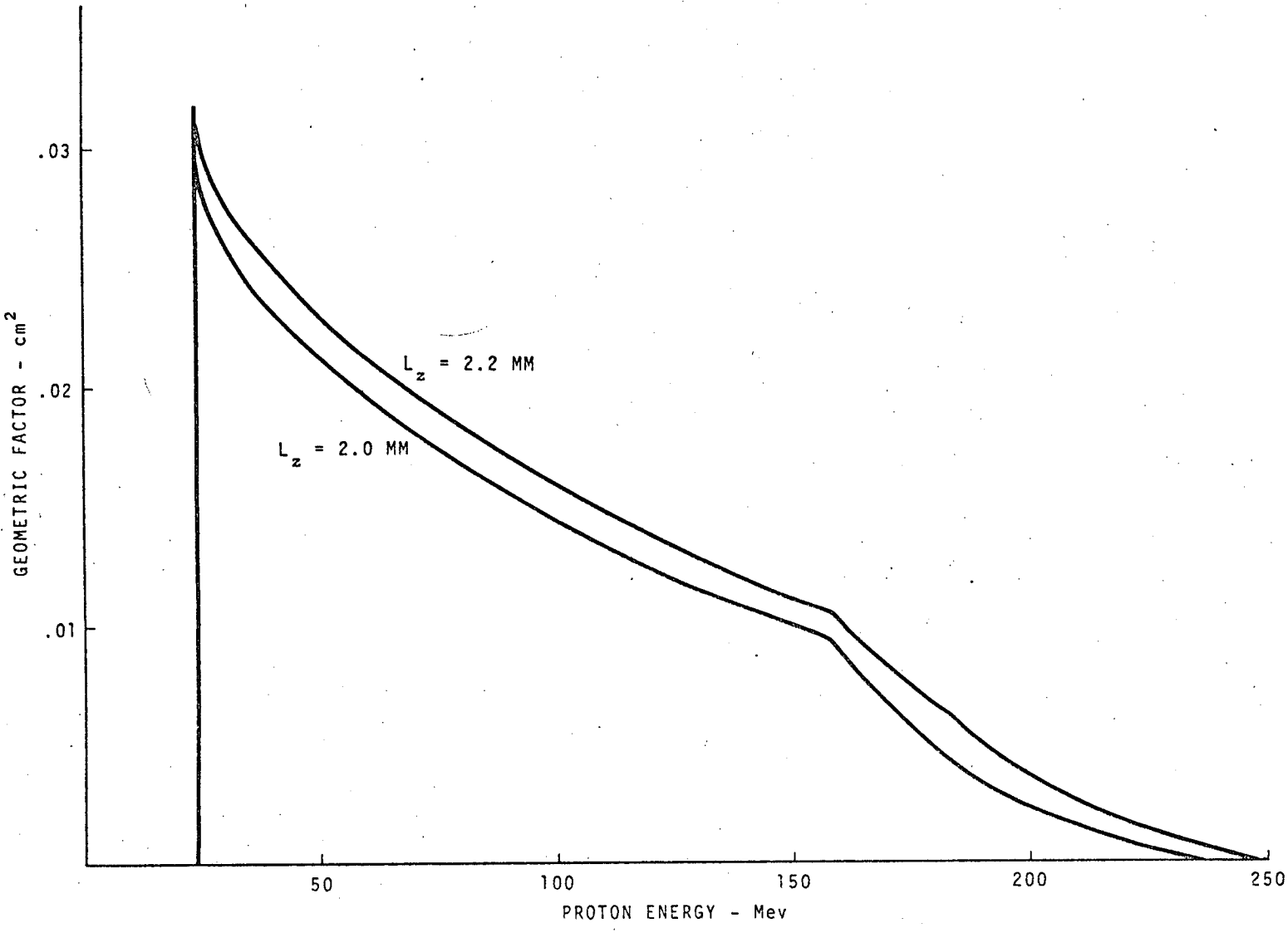

Figure 4. — Geometric Factor, Channel 3, Protons.

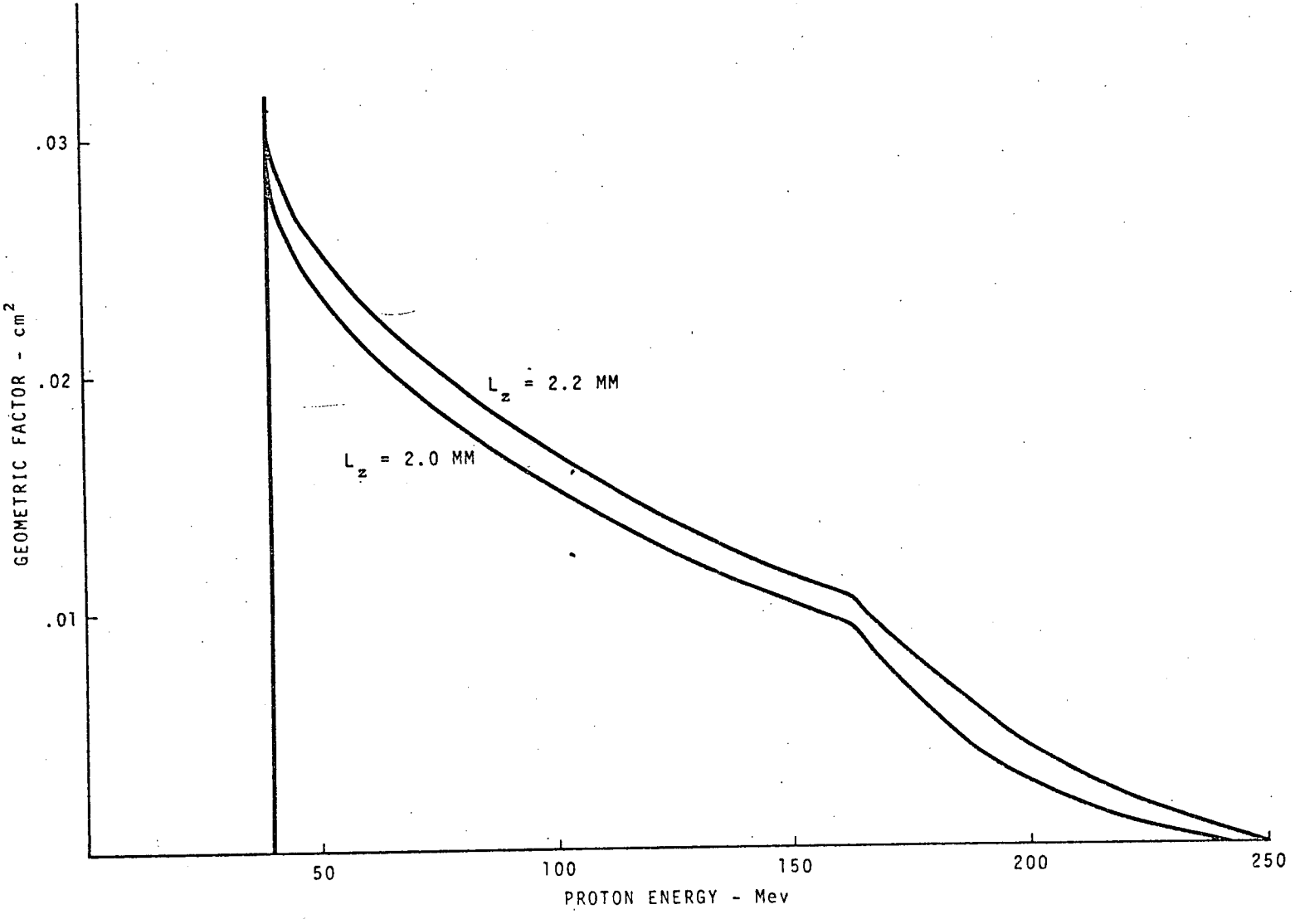

Figure 5. — Geometric Factor, Channel 4, Protons.

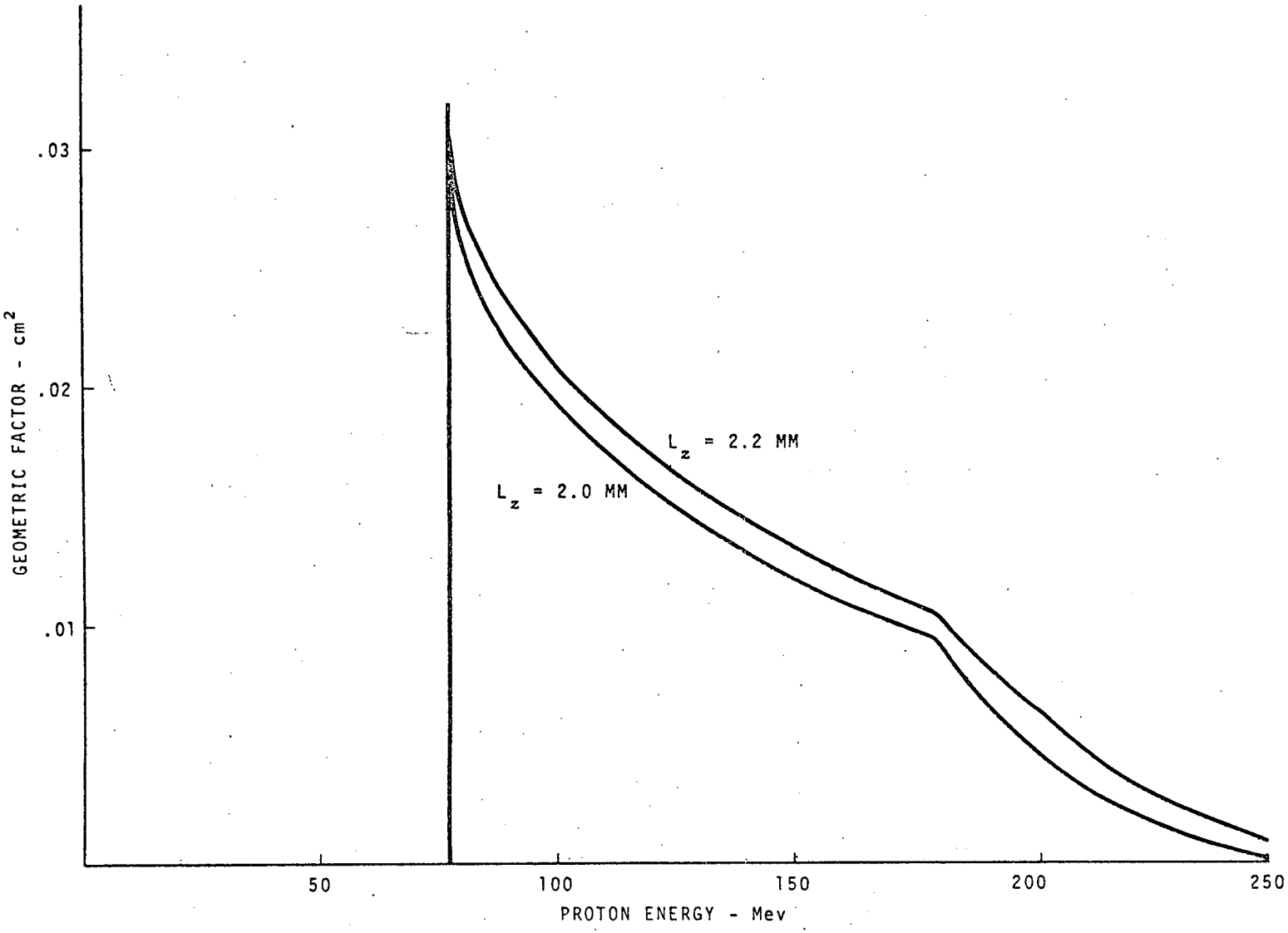

Figure 6. — Geometric Factor, Channel 5, Protons.

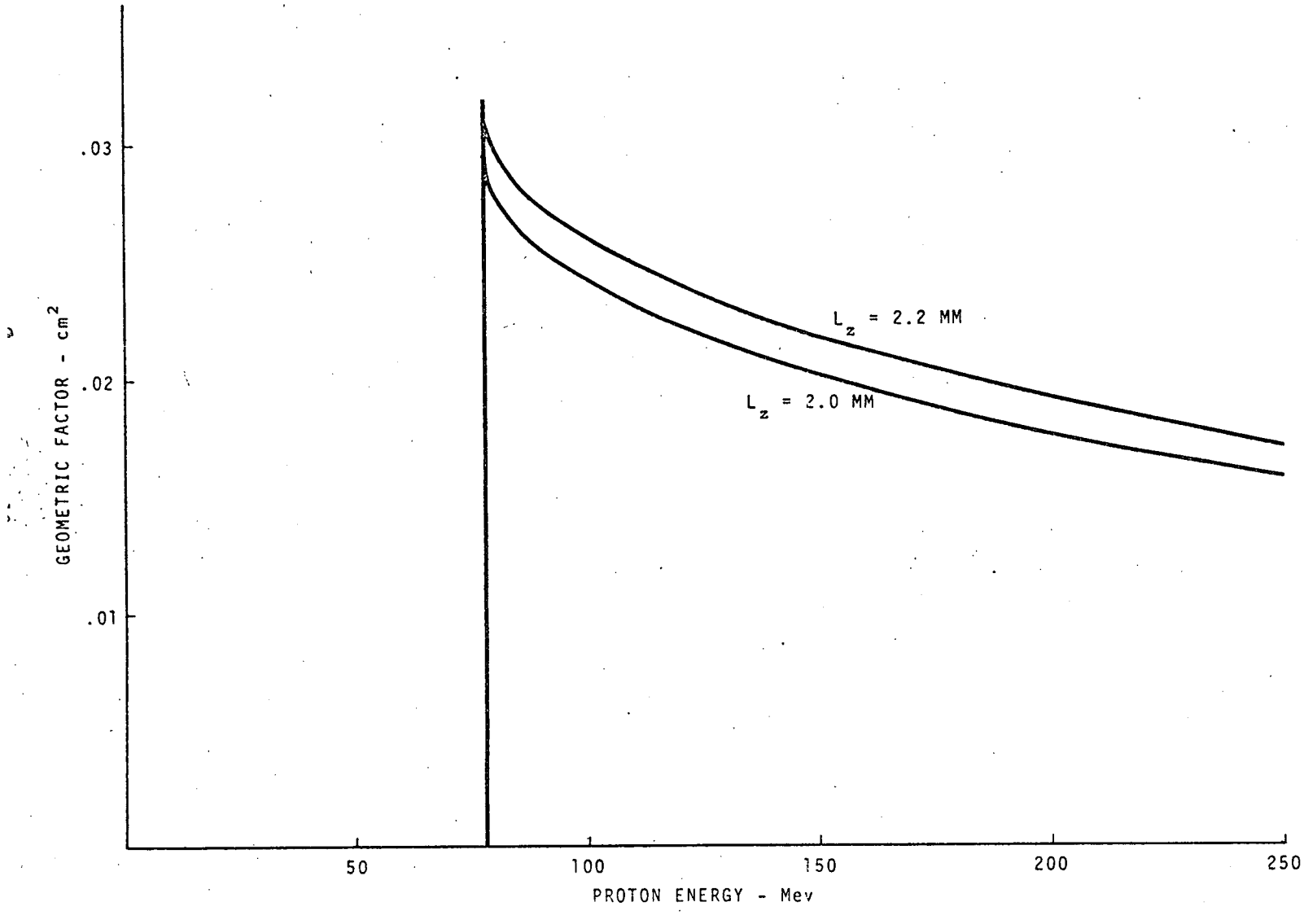

Figure 7. — Geometric Factor, Channel 6, Protons.

4.0 EXPERIMENTAL DETERMINATION OF RESPONSE FUNCTIONS

An experimental program was undertaken to verify the calculated proton response and to determine the electron response of the EPS.

4.1 Proton Calibration

Protons were obtained at two cyclotrons for the purpose of calibrating the EPS. Low energy protons, from 8 MeV to 43 MeV, were obtained from the Texas A&M University Variable Energy Cyclotron, College Station, Texas. Higher energy protons, from 52 MeV to 153 MeV, were obtained from the fixed energy Harvard University Synchrocyclotron, Cambridge, Massachusetts. Since the particles from a cyclotron, after extraction, are essentially monoenergetic and monodirectional, measurements were made at several discrete energies and at various angles with respect to the detector. In each case, specific energies were obtained by degrading and scattering selected beam energies. The angles were obtained by rotating the shielded detector in the beam. The symmetry of a cube was utilized to minimize the number of angles. Five angles were selected: normal to the front face, normal to a side face, a front edge, a side edge, and a corner.

A collimated high quality 2.0 mm thick lithium-drifted silicon detector was used for flux calibration. The collimator was a simple brass collimator with sufficient thickness to stop the incident protons and with a hole large enough to make any collimator effects insignificant relative to the transmitted beam. Commercial electronics, suitable for use

4.0 Continued

with high quality solid state detectors, were utilized to amplify and count the detector output pulses. A bias of 500 V was applied to the detector and a pulse shaping time constant of 1.0 μsec was utilized in the amplifier. At Texas A&M a pair of stacked 5.0 mm lithium-drifted silicon detectors, operated at 1000 V, were used for proton energy determination. A 4096 channel pulse height analyzer was used to record the output spectra of the detectors. In order to prevent pile-up of pulses in the electronic apparatus a low flux of protons was maintained. Energy calibration was achieved at Harvard University by range measurements utilizing calibrated aluminum foils and range-energy tables.

For each beam energy configuration, a calibration run was made to determine the beam energy and particle flux of the experimental location. Afterwards, the calibration detector was replaced with the EPS calibration sensor for an experimental run. The EPS calibration sensor consists of one of five shields made to the same specifications as the shields used on the flight system and a 2.0 mm cubical detector selected from the test detectors undergoing testing and evaluation. A special electronics system was built to have the same specifications as the preamplifier and amplifier of the flight system plus a special pulse stretcher to allow analysis by commercial electronics. The detector

4.0 Continued

was operated at a bias of 350 V and a pulse shaping time constant of 360 nsec was used. The multichannel analyzer was used to record the output spectra of the detector. A fast threshold monitor was used to provide a correction for pulses lost due to analysis dead time. Spectra were recorded for each of several energies with each shield. The pulses greater than 2.0 MeV (and 1.0 MeV in channel 6) were totalized in each spectrum and divided by the proton flux to provide the response of each angle. The responses for each of the several angles were weighed according to the solid angles they represented and summed to give a synthesized 2π steradian response. The normalized responses are plotted in Figures 8 - 13. Since the two detectors used were both close to 2.20 mm thick (L_Z), the experimental values were normalized to that value and plotted along with the analytic response for the same size detector for comparison. The normalized data values are given in Table II for each of the channels.

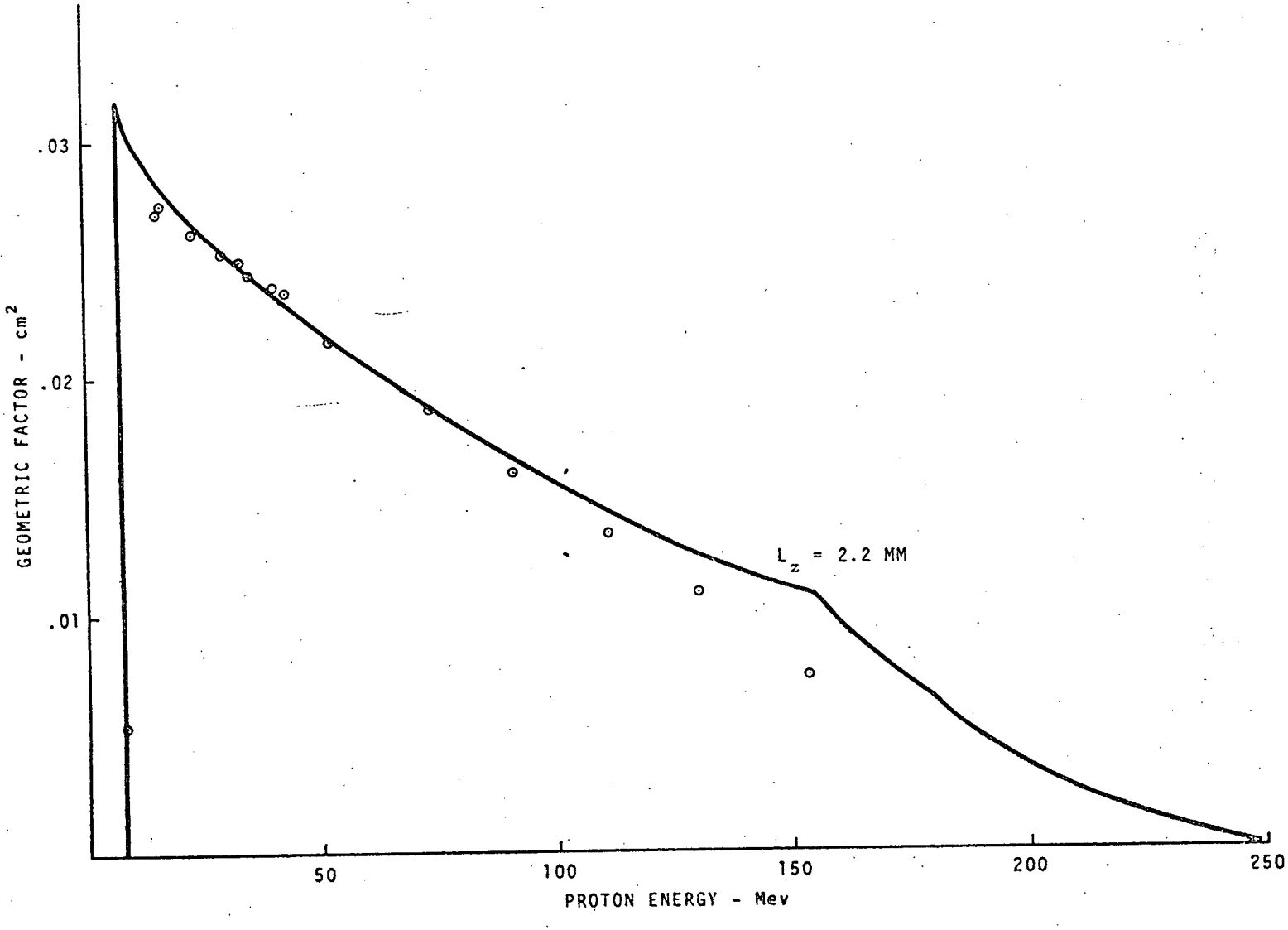

Figure 8. — Geometric Factor, Channel 1, Protons.

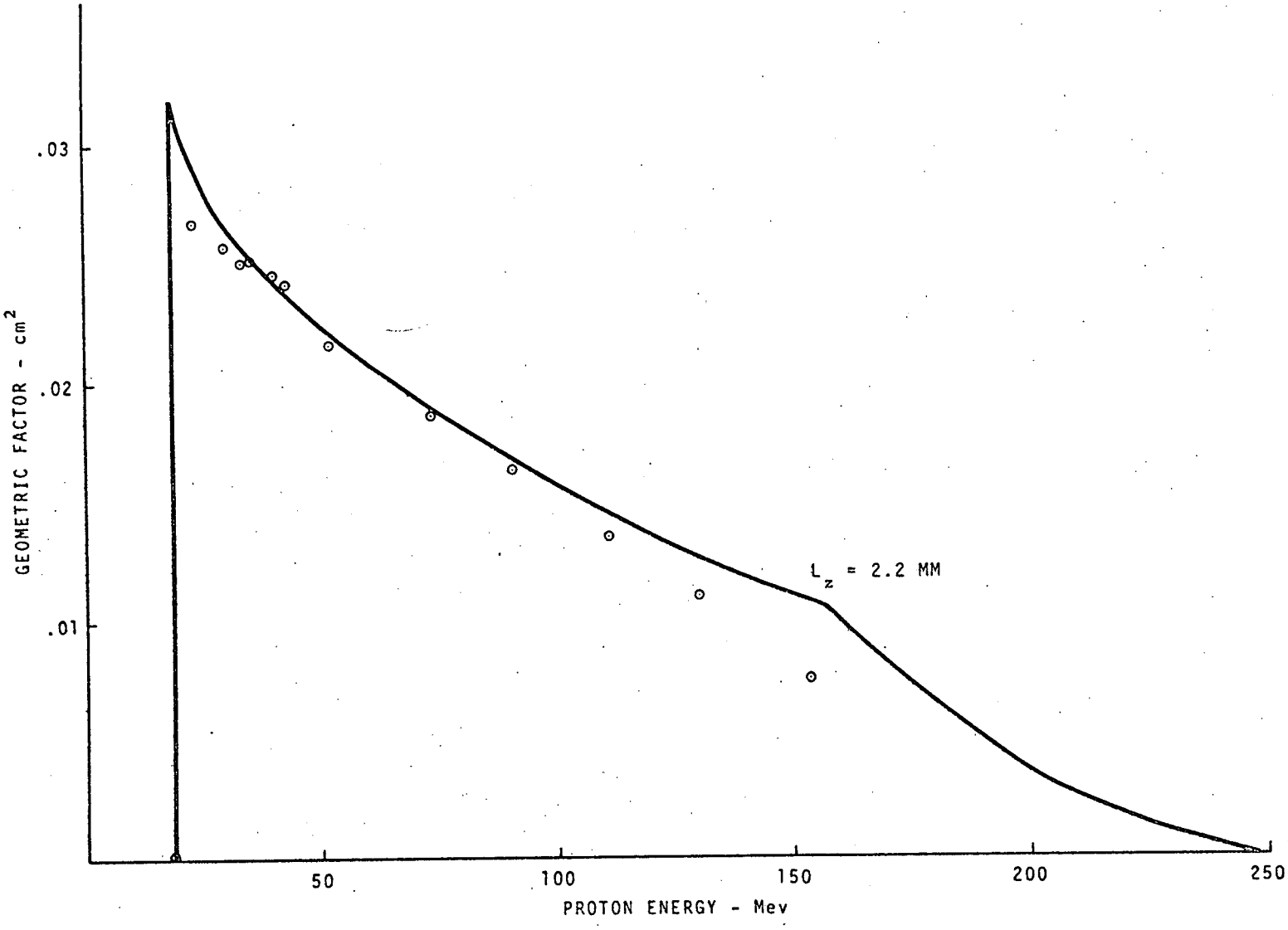

Figure 9. — Geometric Factor, Channel 2, Protons.

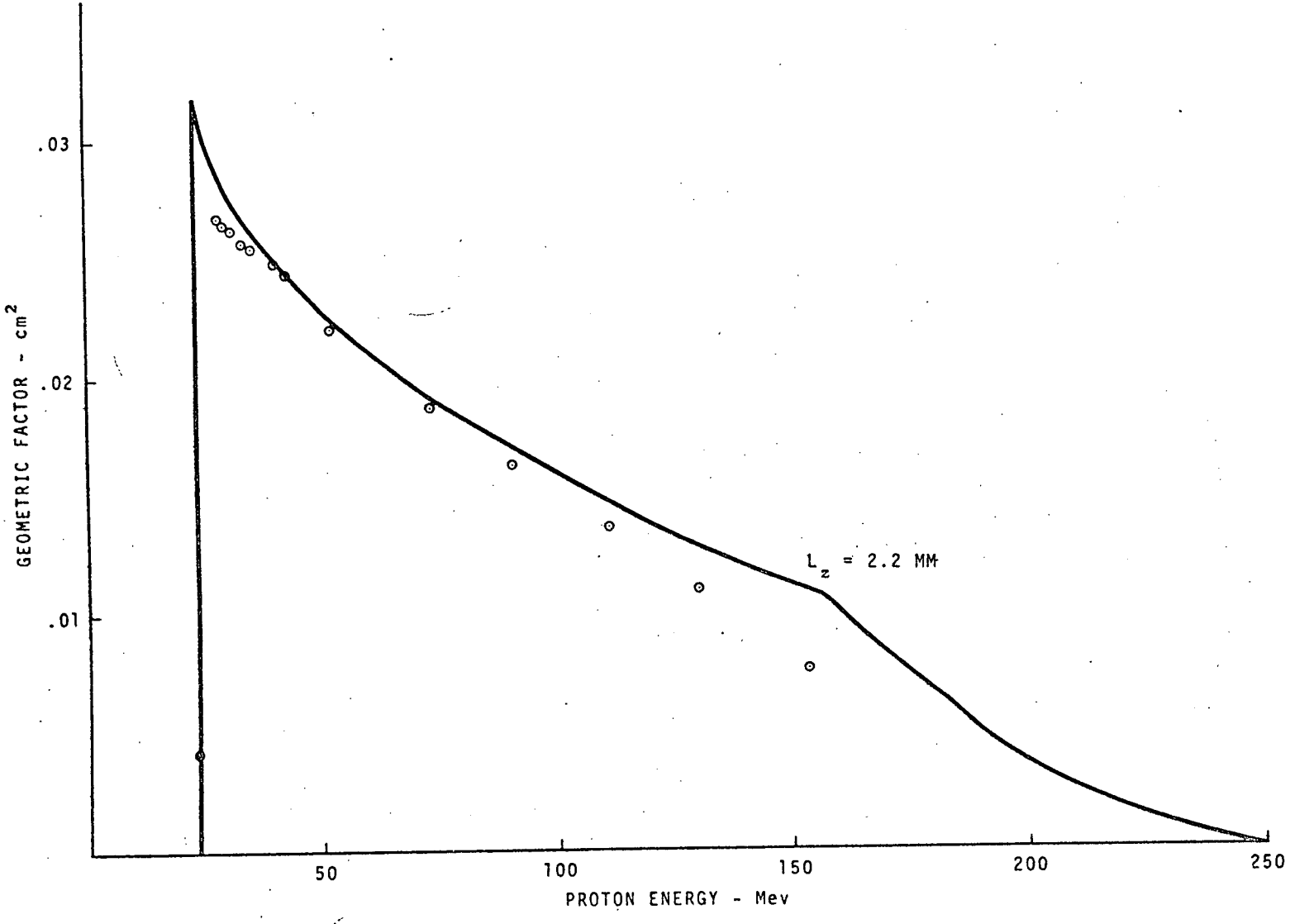

Figure 10. — Geometric Factor, Channel 3, Protons.

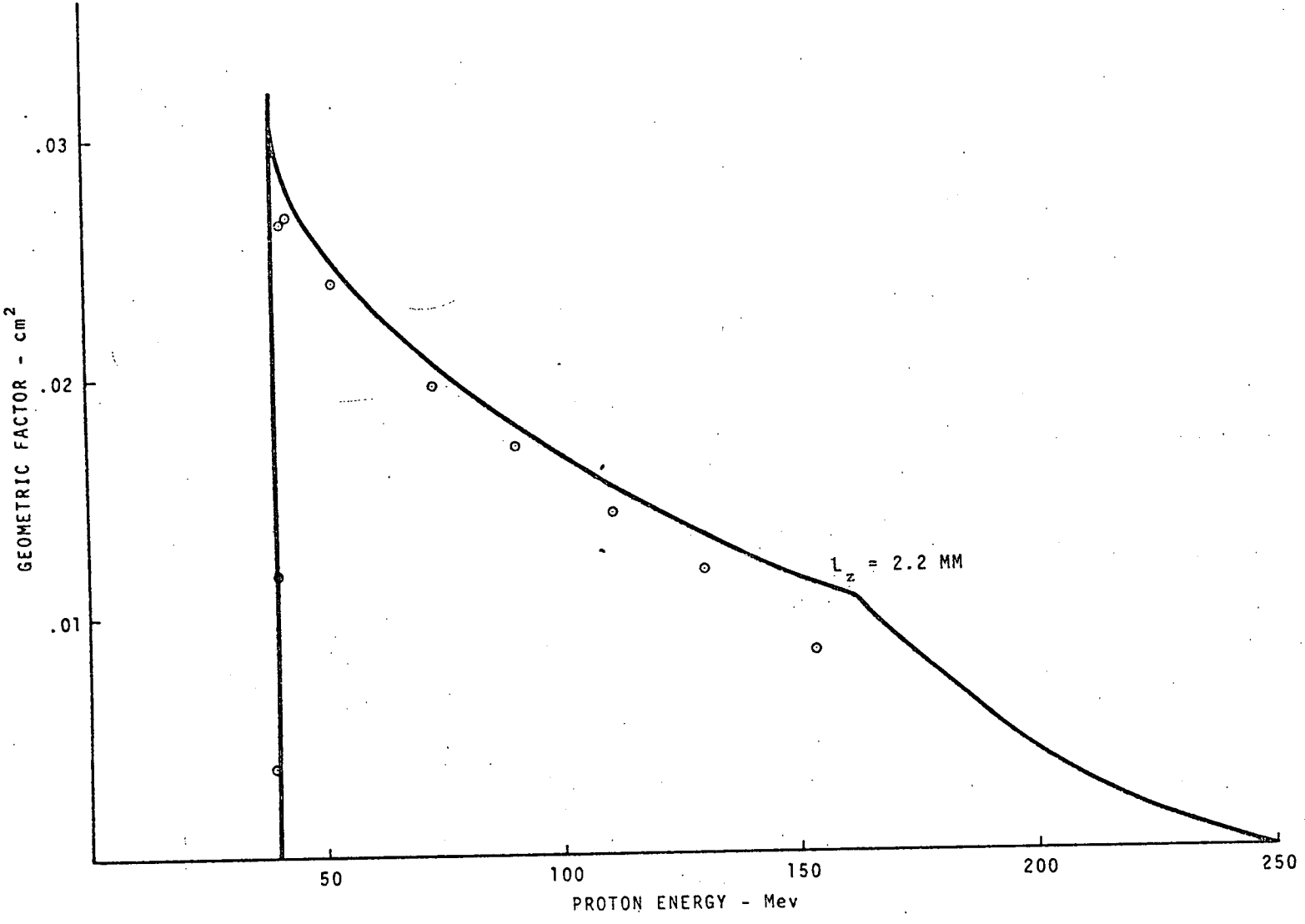

Figure 11. — Geometric Factor, Channel 4, Protons.

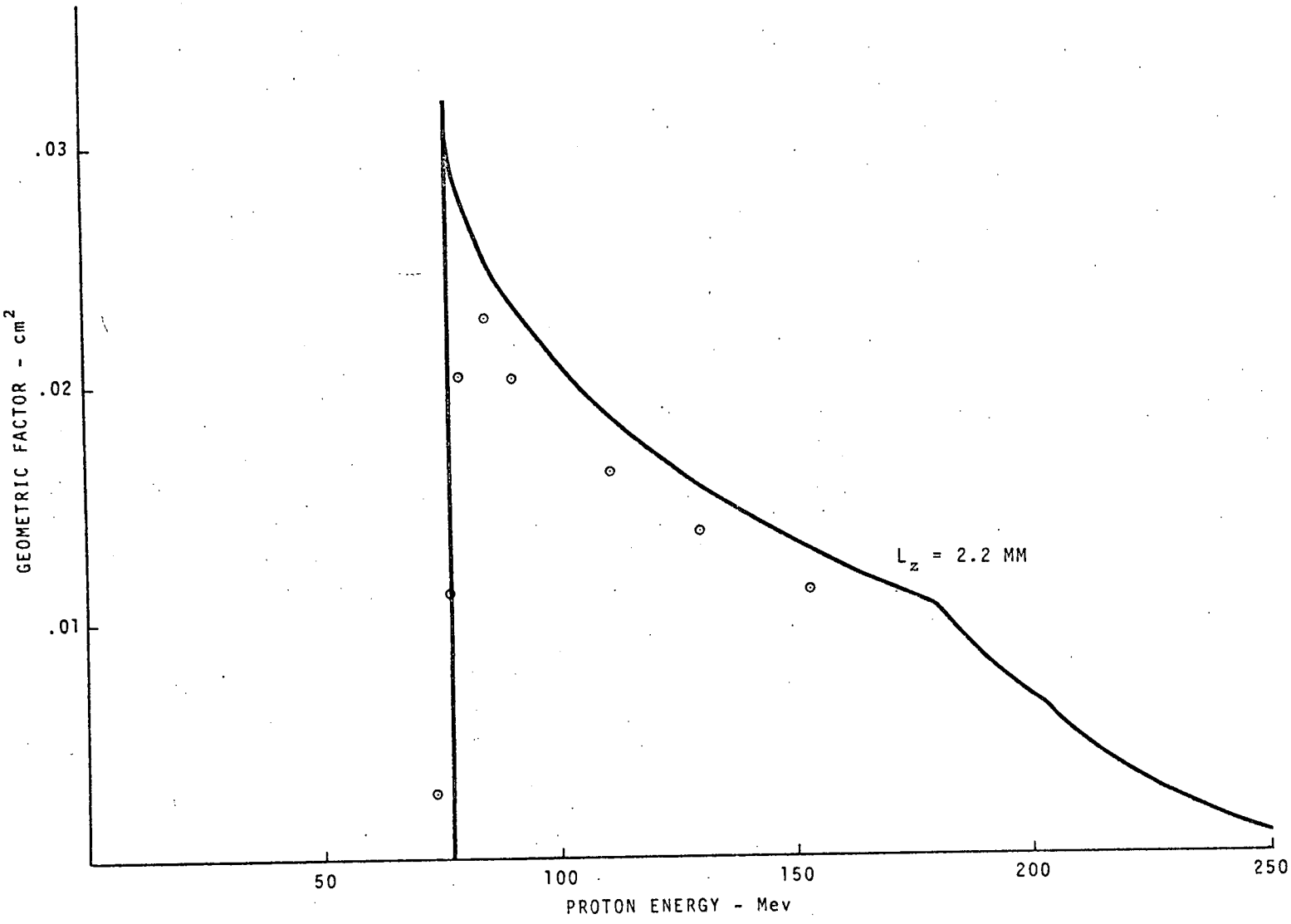

Figure 12. – Geometric Factor, Channel 5, Protons.

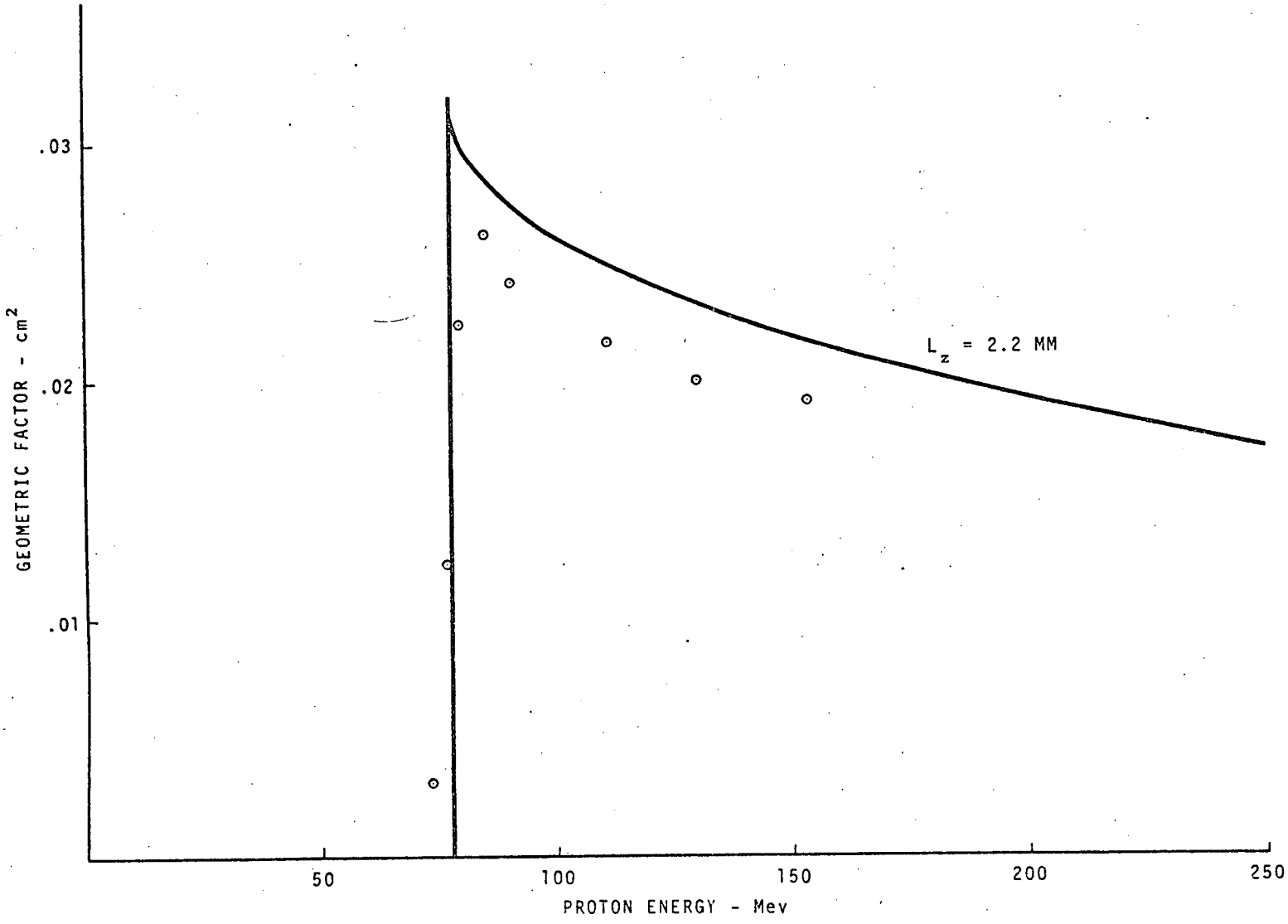

Figure 13. — Geometric Factor, Channel 6, Protons.

Table II Experimental Geometric Factors - Protons

Proton Energy	EPS Channel 1	2	3	4	5	6
153.4	.0073	.0075	.0076	.0084	.0112	.0192
130.0	.0108	.0110	.0110	.0118	.0137	.0200
111.0	.0133	.0135	.0136	.0142	.0162	.0216
90.4	.0159	.0163	.0163	.0170	.0202	.0241
85.0					.0227	.0261
79.4					.0203	.0224
76.8					.0112	.0123
73.2	.0183	.0186	.0187	.0196	.0028	.0031
52.0	.0215	.0215	.0220	.0239		
42.9	.0236	.0241	.0244	.0267		
41.2				.0264		
40.1	.0238	.0245	.0246	.0118		
38.9				.0037		
35.3	.0243	.0251	.0254			
33.5	.0249	.0250	.0257			
31.3			.0262			
29.7	.0252	.0257	.0264			
28.2			.0267			
23.1	.0261	.0267	.0042			
21.4	.0260					
18.0		.0001				
16.3	.0273					
15.4	.0269					
8.5	.0053					

4.1 Continued

Examination of the figures shows that the agreement between the analytic and experimental curves is, in general, good. There appear to be three sources of significant disagreement.

a. The experimental values are low in the higher energy region of all channels. This disagreement apparently stems from the finite resolution of the detector and electronics system with a resulting loss of counts below the 2.0 MeV discriminator level. The effect worsens at higher energies because less energy is deposited in the detector by higher energy protons and hence a greater percentage of the proton counts is lost below the fixed discriminator level.

b. The agreement between the analytic and experimental values in the intermediate energy regions gradually worsens from the low energy channels to the high energy channels. This disagreement apparently stems from the fact that the shield thickness increases with channel number, giving rise to greater proton scattering. Since the scattering paths vary widely depending upon the point of incidence on the shield, the protons scattered away from the detector are not totally compensated for by protons scattered into the detector. This effect is insignificant for channels 1 and 2, is approximately 2% for channel 3, is approximately 5% for channel 4, and is approximately 13% for channels 5 and 6.

c. The third source of disagreement between the analytic and experimental values lies in the region immediately above the threshold for each channel. The finite resolution of the detector and electronics system, and the straggling of the protons prevents the experimental values from following the sharp rise of the analytic values. The apparent slope of the threshold in channels 5 and 6 is due to the energy broadening of the cyclotron beam resulting from having to degrade the beam energy from 157 MeV to the threshold energy of 77 MeV.

The impact of the disagreement between the experimental and analytic response functions can be determined by calculating the response of each to a typical proton anomaly spectrum. Figure 14 shows such a differential proton spectrum for the Skylab orbit integrated over a typical day. Calculation of the response of an EPS channel requires a point by point multiplication of the channel response function times the differential proton spectrum and integrating. The results of these calculations are shown in Figures 15 - 20. Each figure shows the differential count spectrum utilizing the analytic response function (upper curve) and the experimental response function (lower curve). Table III shows the number of counts determined for each channel utilizing both response functions.

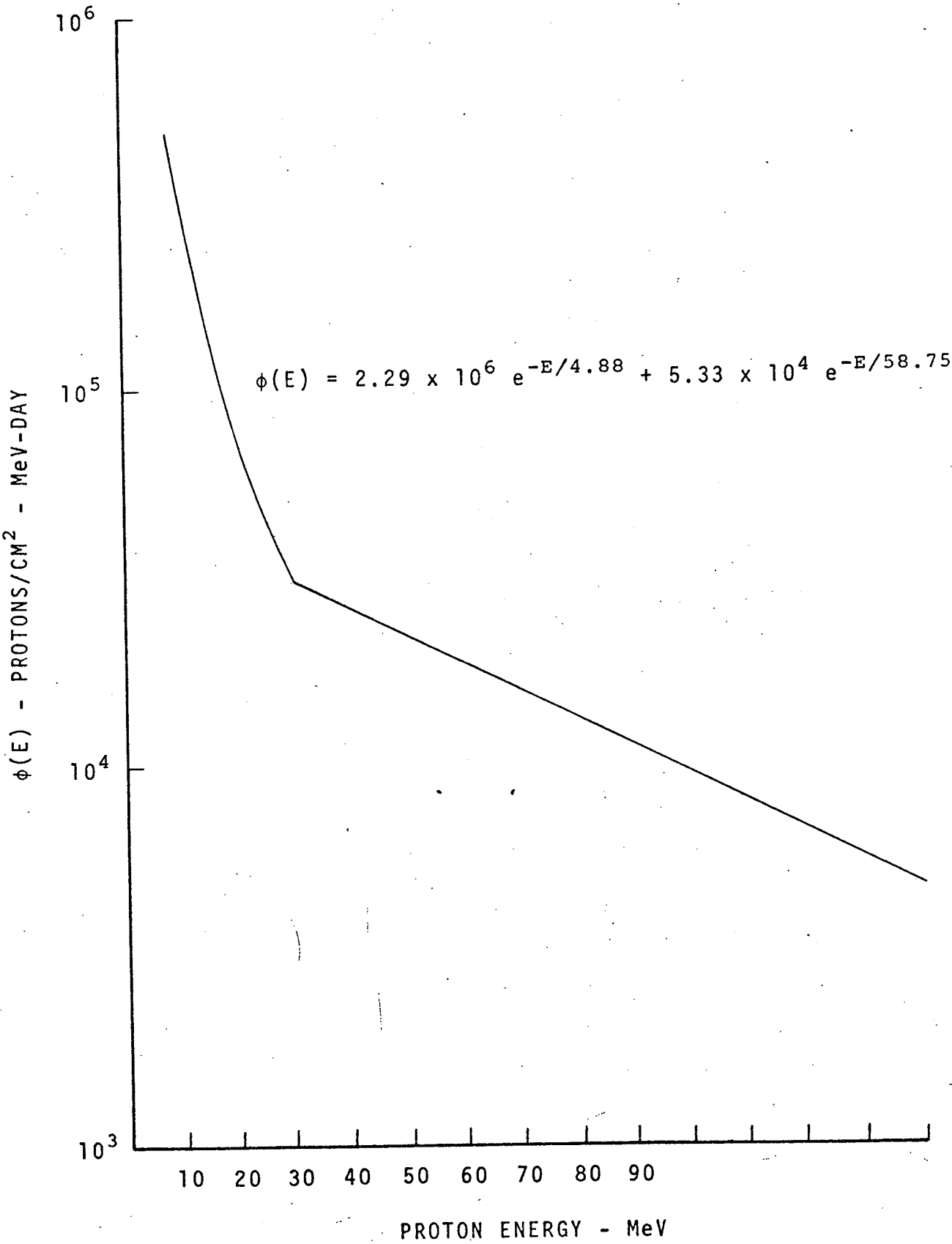

Figure 14. — Differential proton flux at 235 nautical miles.

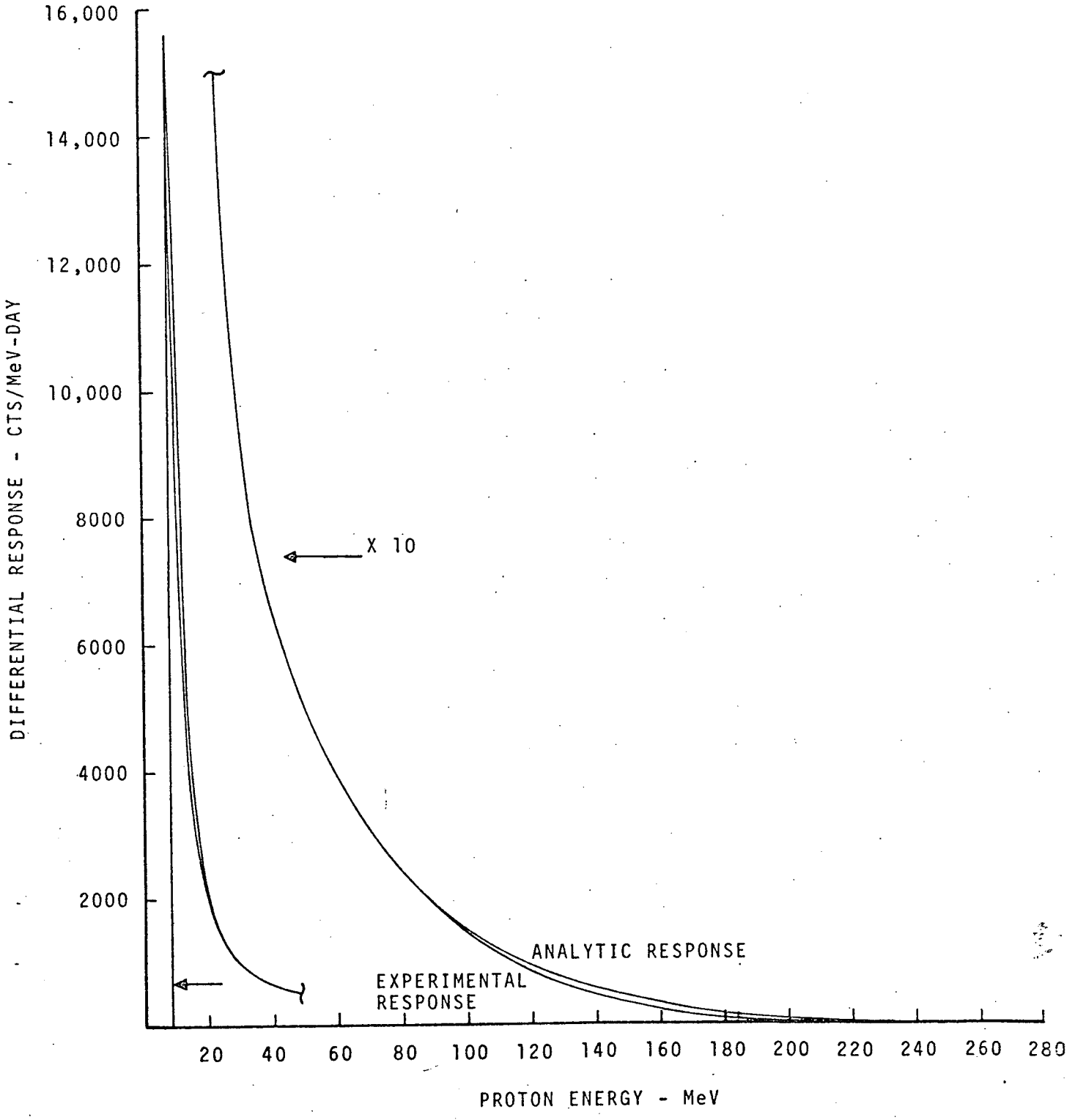

Figure 15. — Differential response to orbit spectrum, channel.

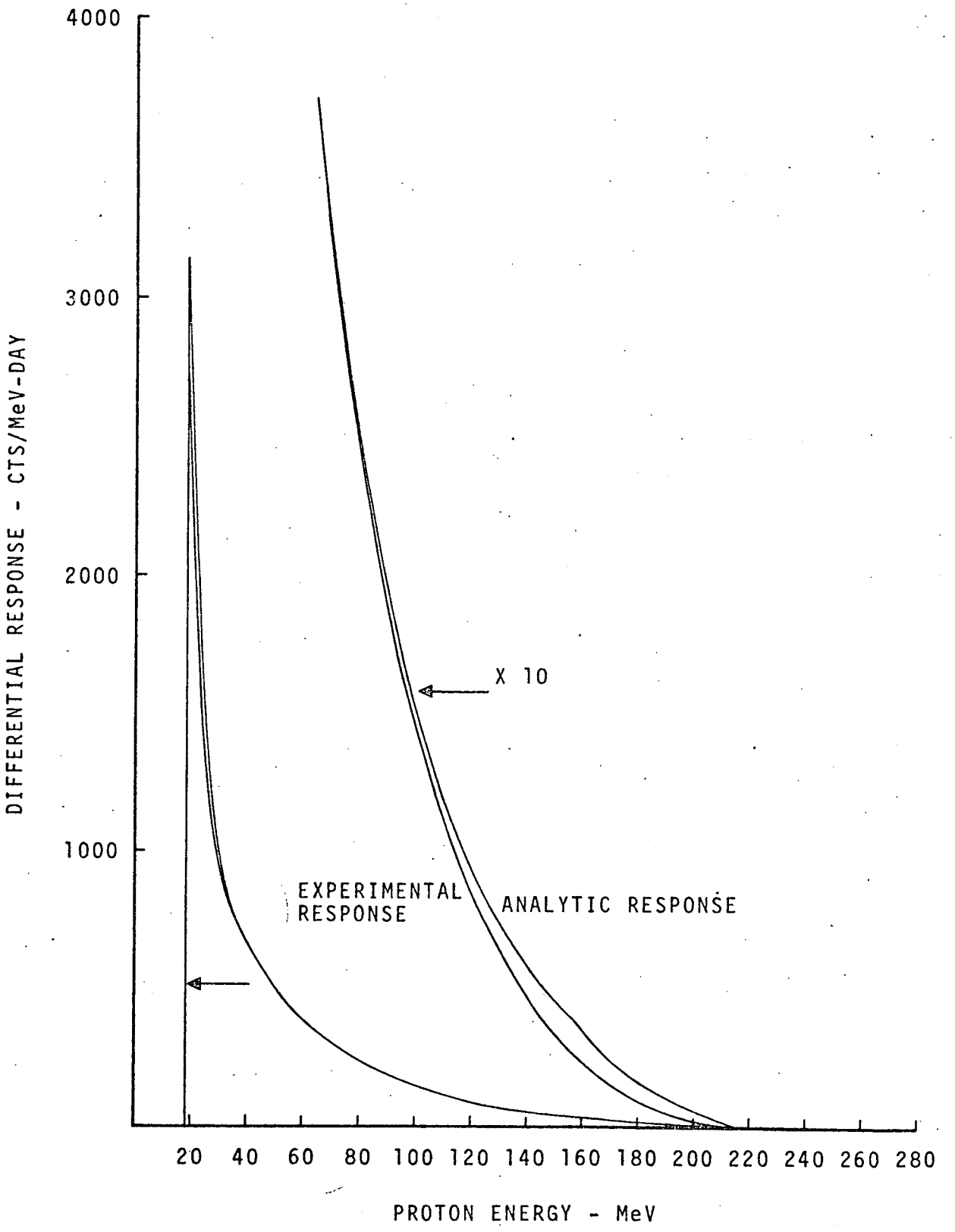

Figure 16. — Differential response to orbit spectrum, channel 2.

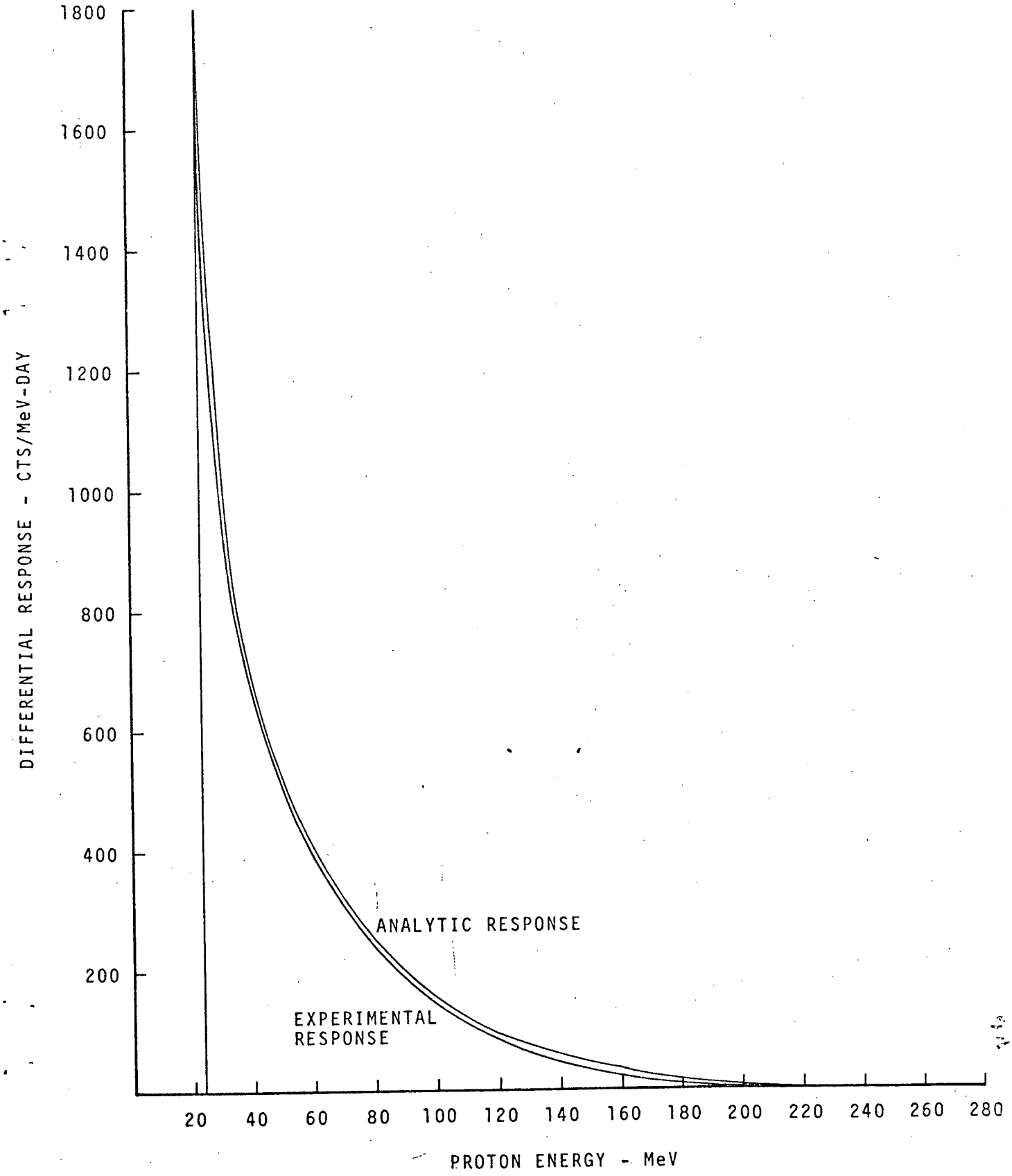

Figure 17. — Differential response to orbit spectrum, channel 3.

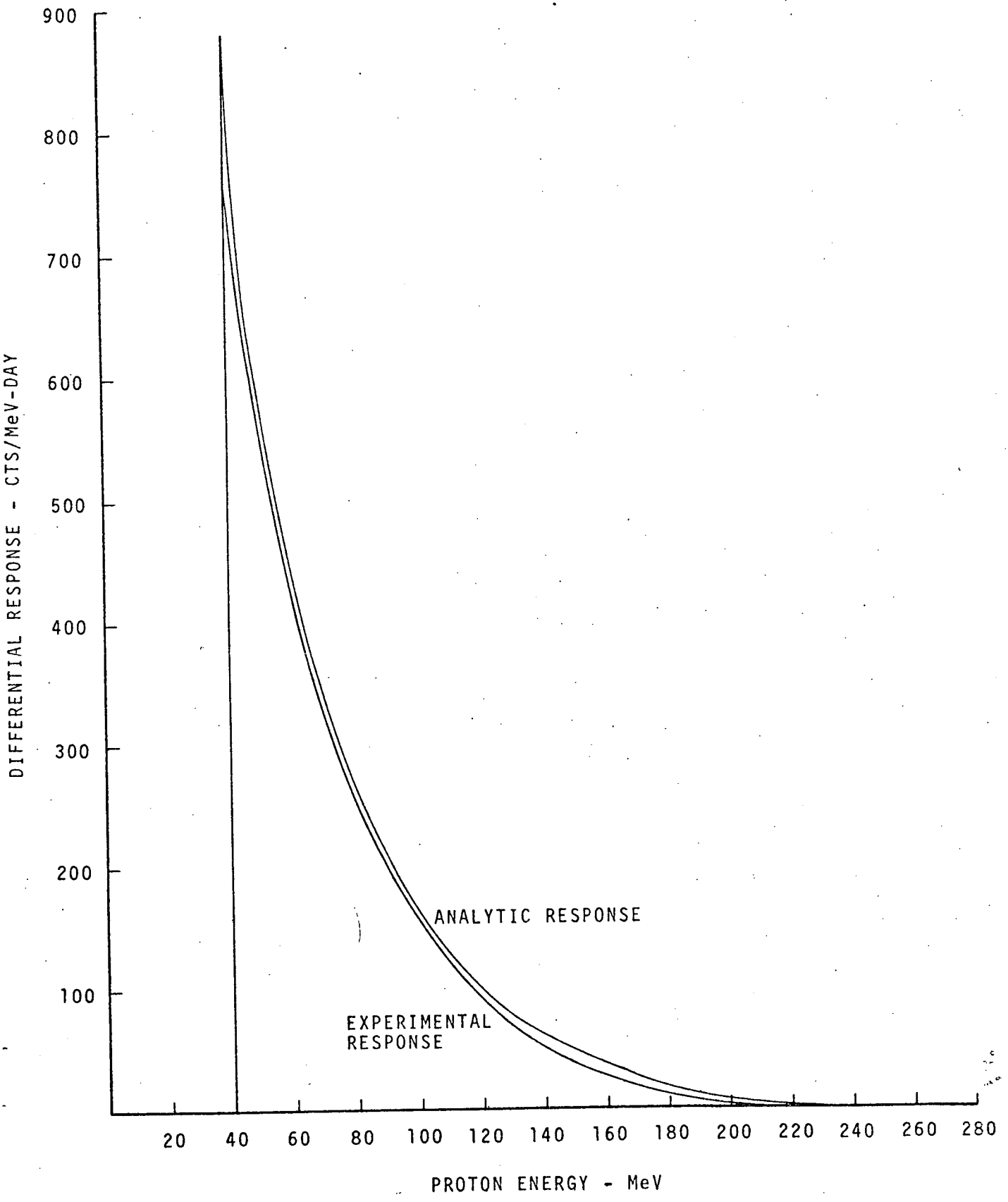

Figure 18. – Differential response to orbit spectrum, channel 4.

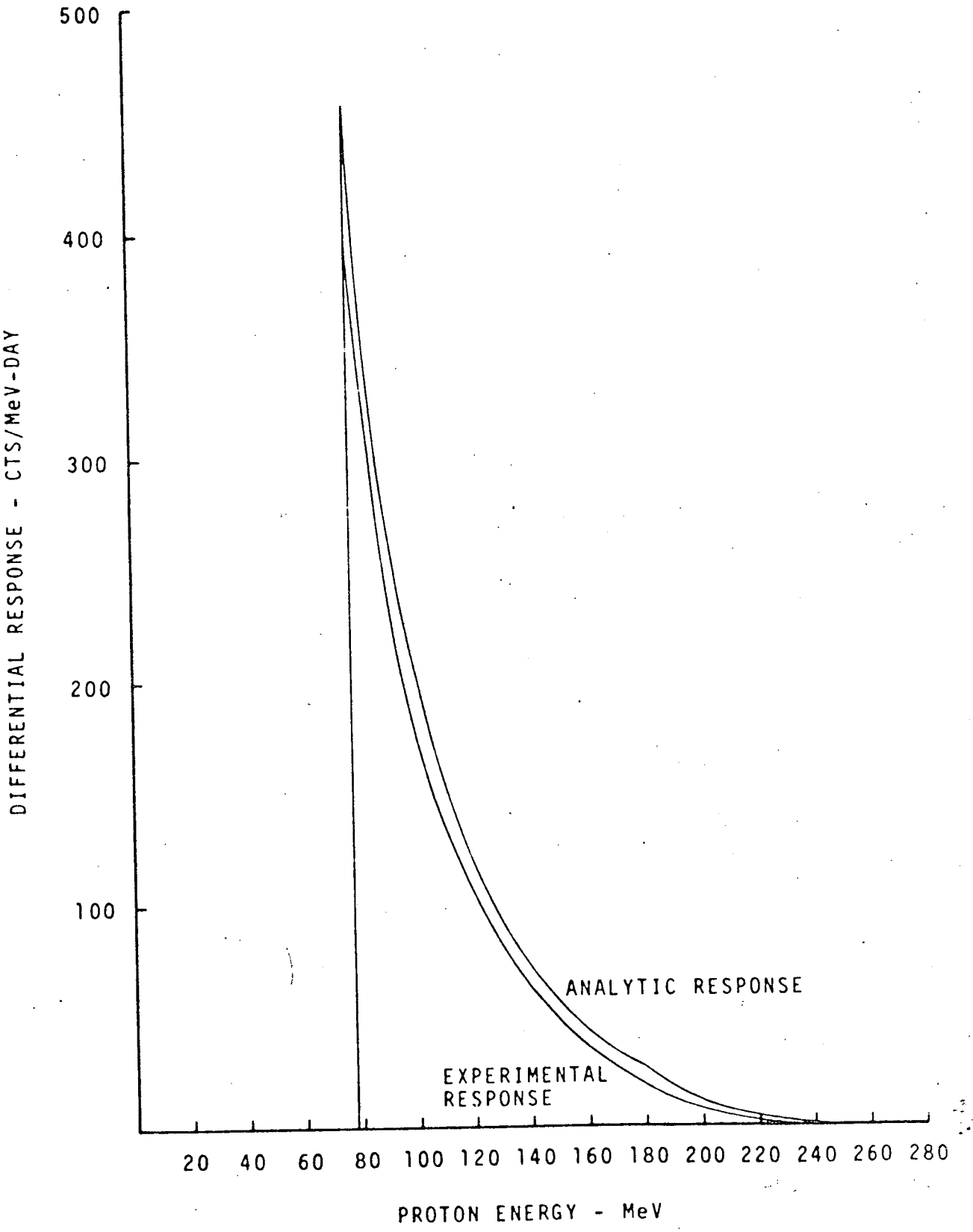

Figure 19. – Differential response to orbit spectrum, channel 5.

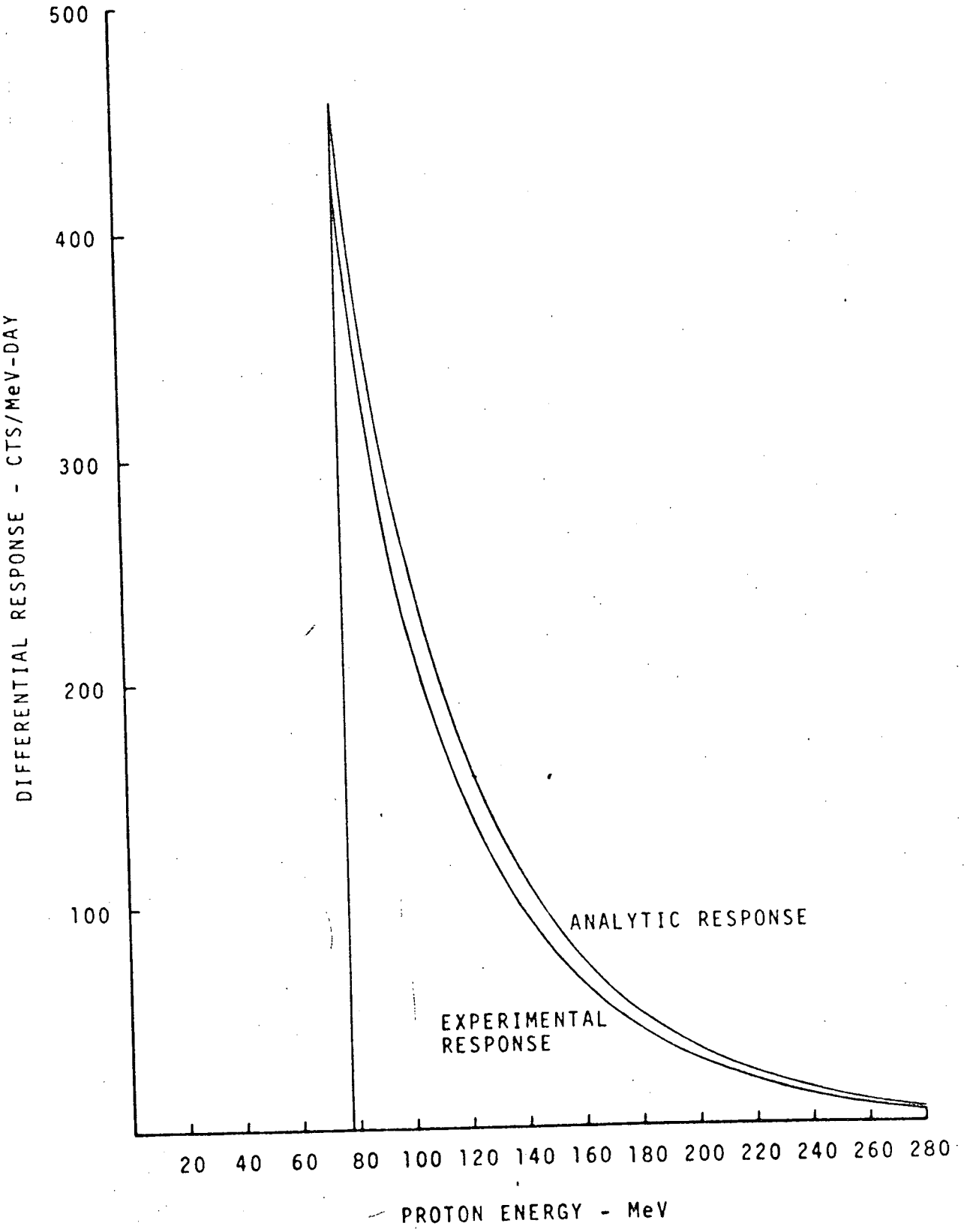

Figure 20. – Differential response to orbit spectrum, channel 6.

Table III EPS Response to Orbit Spectrum

Channel	Analytic Response counts/day	Experimental Response counts/day	Ratio Exp/Analytic
1	121008	115288	0.953
2	54283	51276	0.945
3	44603	41603	0.933
4	29011	26975	0.930
5	14133	12267	0.868
6	19871	17480	0.880

4.2 Proton Channel Errors

Four major sources contribute to the system errors for the proton channels of the EPS:

a. measurement of the detector dimensions,

b. measurement of the proton flux during the calibration,

c. variation in the electronics, and

d. variation in the response of the detectors available for use in the flight systems.

Repeated measurements on a group of detectors indicated that the error made in determining a detector dimension is approximately 2%. Combining the errors in quadrature for the three dimensions gives an overall error due to dimensional uncertainty of approximately 4%. Measurement of the proton flux during calibration was estimated to have an error of approximately 5%. The overall variation in the response due to the electronics is estimated to be 5%. The last error is due to the variation in the response of all the detectors constituting the population from which the flight detectors will be chosen. In an effort to approximate the future population of detectors, a group of 26 detectors were given exhaustive tests to determine the survival rate and response of available detectors. Of the original group, only 21 survived the tests and continued to function as nuclear detectors. All of the surviving detectors were irradiated with high energy protons in order to estimate their variation in response. These variations were folded into the response functions which were in turn applied to the proton spectrum of Figure 14 to determine an overall countrate. The range of variation for the detectors is given in Table IV.

Table IV Errors Due to Detector Variances

Channel #	Errors
1	± 3%
2	± 4%
3	± 5%
4	± 6%
5	± 7%
6	± 7%

The effects of the four types of errors are shown in Table V.

Table V Proton Error Summary - Percent

Channel #	1	2	3	4	5	6
Detector Dimension	4	4	4	4	4	4
Calibration	5	5	5	5	5	5
Electronics	5	5	5	5	5	5
Detector Variance	3	4	5	6	7	7
RMS Total	8.7	9.1	9.5	10.1	10.7	10.7

4.3 Electron Calibration

Electrons were obtained at two Van de Graaff accelerators for the purpose of calibrating the EPS. Low energy electrons, from 0.5 MeV to 2.75 MeV, were obtained from the NASA/MSC 3.0 MeV accelerator in Houston, Texas. Higher energy electrons, from 2.0 MeV to 4.2 MeV, were obtained from the 4.0 MeV accelerator at the National Bureau of Standards, Gaithersburg, Maryland. No higher energy electrons were available in useable quantities from nonpulsed machines. As in the case of protons, measurements were made at five selected angles. The values were weighted according to the solid angles they represented and summed to give a synthesized 2π steradian response. The normalized response (L_2 = 2.20 mm) are plotted in Figures 21 - 24 The response for channel 4 is replotted in Figure 25 on an expanded scale to permit better presentation of the data. The normalized data values are given in Table VI for each of the channels. It is assumed that a suitable normalization factor, to correct for variations in detector size, can be determined by taking the ratio of the exposed surface areas of the detectors, as in the case of protons.

The curves for each channel were extrapolated beyond 4.08 MeV by noting certain similarities in the shapes of the curves. First, it was assumed that the response for each channel would peak-out at the same value, i.e. 0.025 cm^2, since the same detector was used in each case.

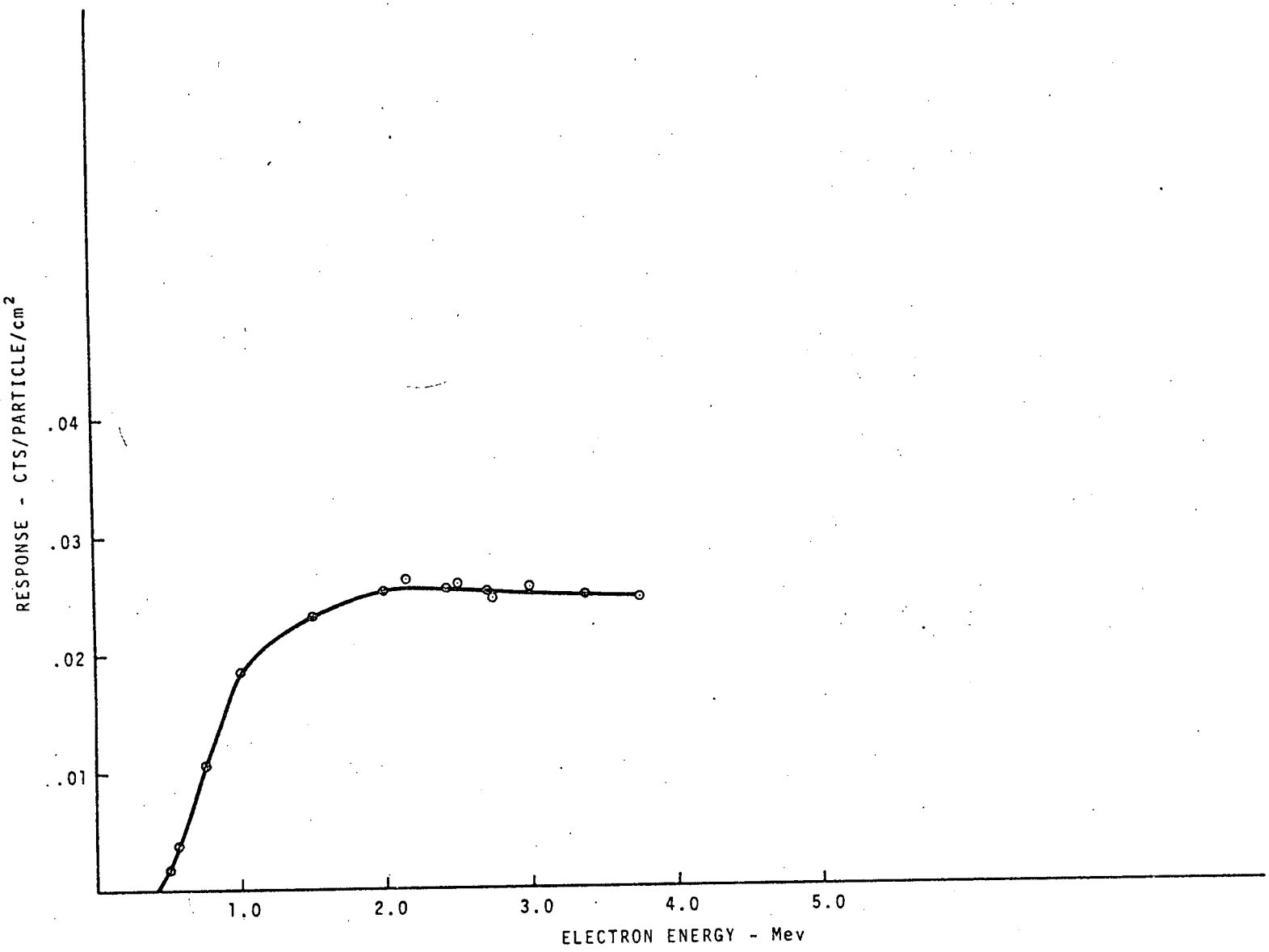

Figure 21. — Omnidirectional Response, Channel 1, Electrons.

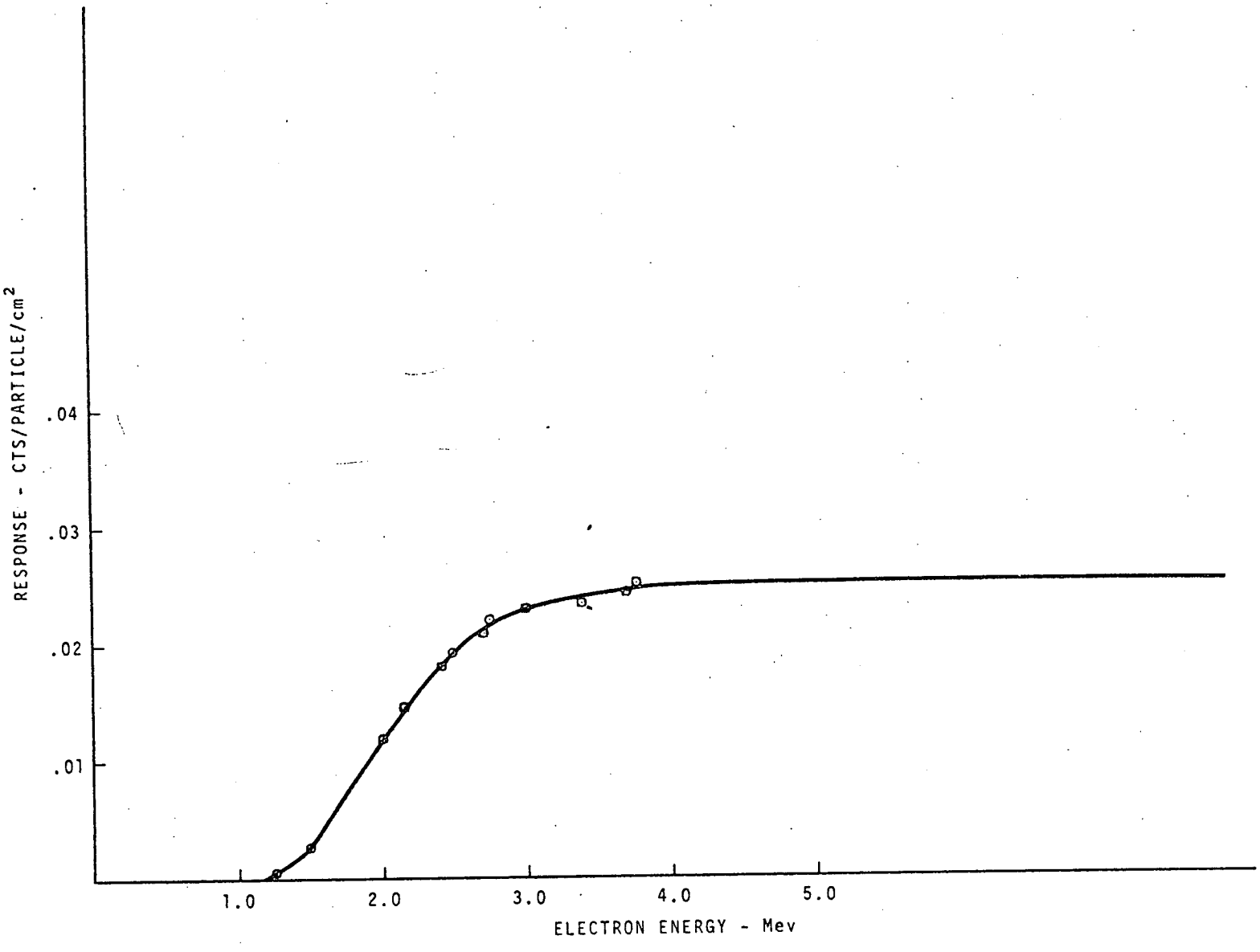

Figure 22. — Omnidirectional Response, Channel 2, Electrons.

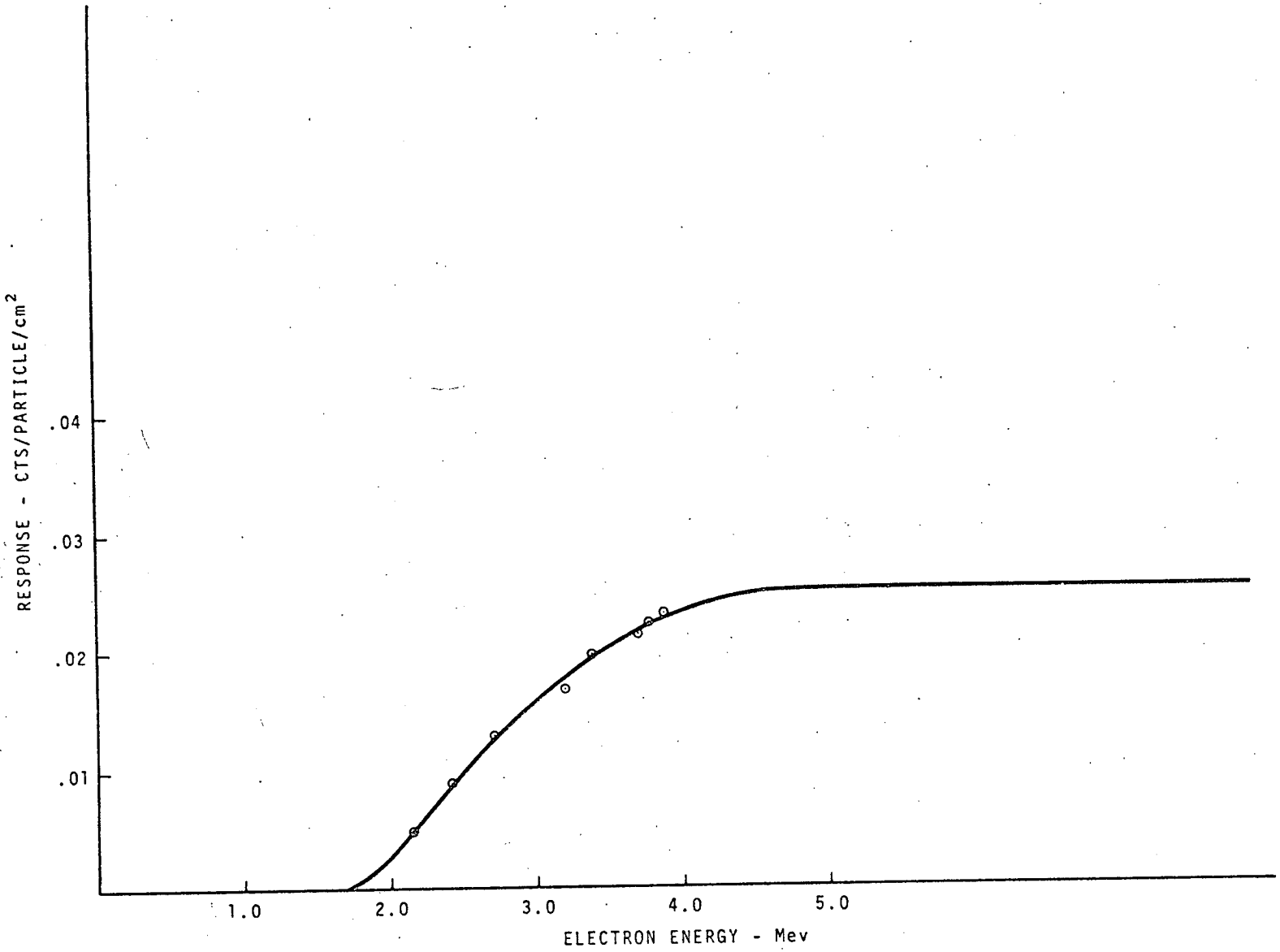

Figure 23. — Omnidirectional Response, Channel 3, Electrons.

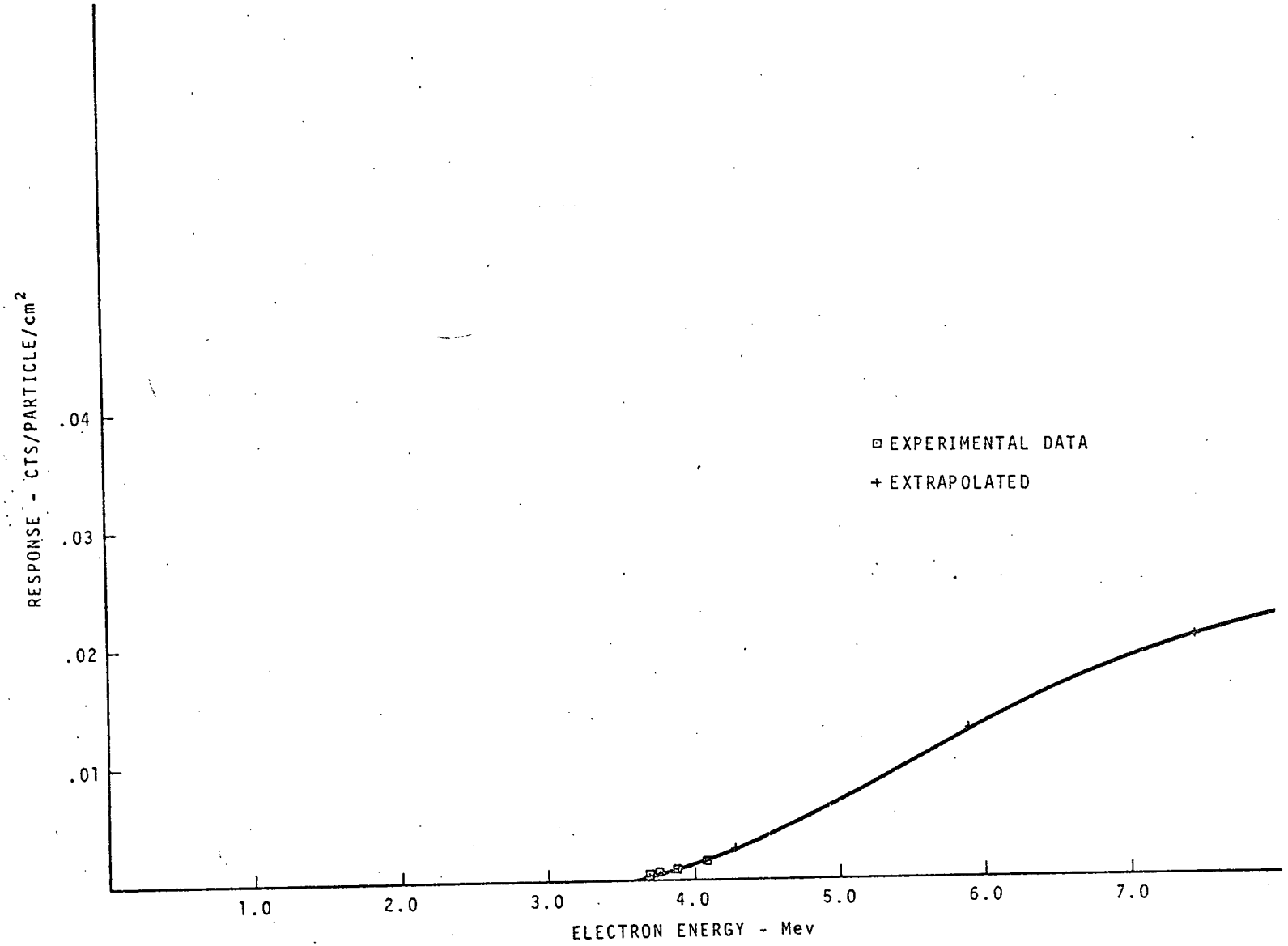

Figure 24. — Omnidirectional Response, Channel 4, Electrons.

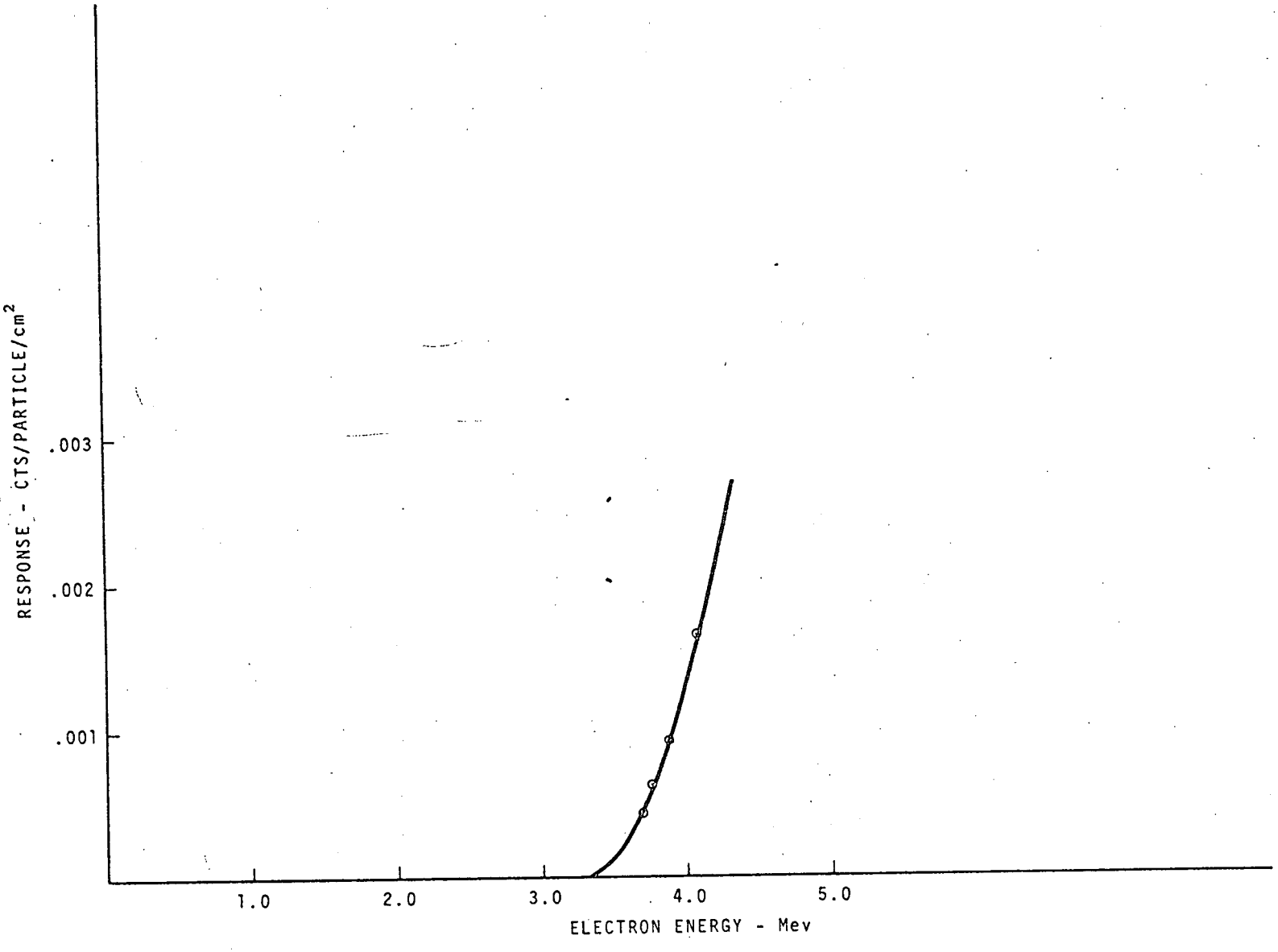

Figure 25. — Omnidirectional Response, Channel 4, Electrons.

4.3 Continued

This assumes that the shape of the leading edge of the curve is due to the shield, and at higher energies the effect diminishes. Taking that maximum, the responses for channels 2 and 3 were normalized to their 10% response energies. It was noted that their shapes were identical. The response for channel 1 did not fit this curve; presumably because the shield was too thin. The response for channel 4 was determined from this normalized curve. For typical values, the energy for 50% response occurs at 1.38 times the energy for 10% response, and the energy for 80% response occurs at 1.74 times the energy for 10% response. Values from the extrapolated curves are given in Table VII.

Table VI Experimental Geometric Factors - Electrons

Electron Energy	EPS Channel 1	2	3	4
4.08				.00165
3.88			.0231	.00092
3.76	.0245	.0249	.0222	.00062
3.69		.0244	.0214	.00043
3.38	.0249	.0234	.0196	
3.00	.0255	.0230	.0166	
2.75	.0247	.0220		
2.71	.0253	.0209	.0128	
2.50	.0258	.0194		
2.42	.0255	.0182	.0089	
2.15	.0261	.0148	.0048	
2.00	.0253	.0120		
1.50	.0231	.00282		
1.25		.00056		
1.00	.0186			
.75	.0106			
.57	.00370			
.50	.00177			

Table VII Omnidirectional Response - Electron

Electron Energy	EPS Channel 1	2	3	4
0.4	.0000			
0.5	.0018			
0.6	.0045			
0.7	.0082			
0.8	.0125			
0.9	.0160			
1.0	.0186			
1.1	.0200	.0000		
1.2	.0210	.0002		
1.3	.0218	.0007		
1.4	.0225	.0015		
1.5	.0231	.0028		
1.6	.0237	.0045	.0000	
1.7	.0242	.0062	.0002	
1.8	.0247	.0082	.0008	
1.9	.0250	.0100	.0015	
2.0		.0120	.0027	
2.1		.0136	.0041	
2.2		.0154	.0055	
2.3		.0168	.0070	
2.4		.0183	.0085	
2.5		.0195	.0100	
2.6		.0205	.0112	
2.7		.0213	.0125	
2.8		.0220	.0137	
2.9		.0225	.0148	
3.0		.0230	.0158	
3.1		.0233	.0168	
3.2		.0236	.0178	

Table VII Omnidirectional Response - Electrons

(Continued)

Electron Energy	EPS Channel 1	2	3	4
3.3		.0238	.0186	
3.4		.0240	.0194	
3.5		.0242	.0202	.0000
3.6		.0244	.0210	.0001
3.7		.0245	.0216	.0004
3.8		.0246	.0223	.0007
3.9		.0247	.0228	.0009
4.0		.0248	.0233	.0013
4.1		.0249	.0237	.0017
4.2		.0250	.0240	.0021
4.3			.0244	.0027
4.4			.0246	.0032
4.5			.0248	.0037
4.6			.0249	.0043
4.7			.0250	.0049
4.8				.0055
4.9				.0060
5.0				.0066
5.1				.0072
5.2				.0078
5.3				.0085
5.4				.0090
5.5				.0096
5.6				.0103
5.7				.0110
5.8				.0116
5.9				.0125

Table VII Omnidirectional Response - Electrons
(Continued)

Electron Energy	Channel 1	2	3	4
6.0				.0130
6.1				.0136
6.2				.0142
6.3				.0147
6.4				.0153
6.5				.0158
6.6				.0163
6.7				.0168
6.8				.0173
6.9				.0178
7.0				.0182
7.1				.0187
7.2				.0191
7.3				.0195
7.4				.0199
7.5				.0203
7.6				.0206
7.7				.0210

4.4 Electron Channel Errors

Three major sources contribute to the system errors for the electron channels of the EPS:

a. measurement of the detector dimensions,

b. measurement of the electron flux during calibration

c. variation in the electronics.

The fourth error source for the proton channels, that is due to variation in response of the detectors, is not significant in the electron channels due to the low discriminator level of 200 keV.

As in the case of the protons, the overall error due to dimensional uncertainties is approximately 4%. Measurement of the electron flux during calibration was estimated to have an error of approximately 5%. The overall variation in the response due to the electronics is estimated to be 5%. Summary of the errors is shown in Table VIII.

Table VIII Electron Error Summary - Percent

Channel #	1	2	3	4
Detector Dimension	4	4	4	4
Calibration	5	5	5	5
Electronics	5	5	5	5
RMS Total	8.1	8.1	8.1	8.1